AMERICAN SOCIETY FOR MICROBIOLOGY | mBio®

RESEARCH ARTICLE

Near-Pan-neutralizing, Plasma Deconvoluted Antibody N49P6 Mimics Host Receptor CD4 in Its Quaternary Interactions with the HIV-1 Envelope Trimer

William D. Tolbert,[a] Dung N. Nguyen,[a] Zahra Rikhtegaran Tehrani,[b,c] Mohammad M. Sajadi,[b,c,d] Marzena Pazgier[a]

[a]Infectious Disease Division, Department of Medicine, Uniformed Services University of the Health Sciences, Bethesda, Maryland, USA
[b]Division of Vaccine Research, Institute of Human Virology, University of Maryland School of Medicine, Baltimore, Maryland, USA
[c]Division of Clinical Care and Research, Institute of Human Virology, University of Maryland School of Medicine, Baltimore, Maryland, USA
[d]Department of Medicine, Baltimore VA Medical Center, Baltimore, Maryland, USA

William D. Tolbert and Dung N. Nguyen contributed equally to this work. Author order was determined on the basis of seniority.

ABSTRACT The first step in HIV-1 entry is the attachment of the envelope (Env) trimer to target cell CD4. As such, the CD4-binding site (CD4bs) remains one of the few universally accessible sites for antibodies (Abs). We recently described a method of isolating Abs directly from the circulating plasma and described a panel of broadly neutralizing Abs (bnAbs) from an HIV-1 "elite neutralizer" referred to as patient N49 (N49 Ab lineage [M. M. Sajadi, A. Dashti, Z. R. Tehrani, W. D. Tolbert, et al., Cell 173:1783–1795.e14, 2018, https://doi.org/10.1016/j.cell.2018.03.061]). Here, we describe the molecular details of antigen recognition by N49P6, an Ab of the N49 lineage that recapitulates most of the neutralization breadth and potency of the donor's plasma IgG. Our studies done in the context of monomeric and trimeric antigens indicate that N49P6 combines many characteristics of known CD4bs-specific bnAbs with features that are unique to the N49 Ab lineage to achieve its remarkable neutralization breadth. These include the omission of the CD4 Phe^{43} cavity and dependence instead on interactions with highly conserved gp120 inner domain layer 3. Interestingly, when bound to BG505 SOSIP, N49P6 closely mimics the initial contact of host receptor CD4 to the adjacent promoter of the HIV-1 Env trimer to lock the trimer in the closed conformation. Altogether, N49P6 defines a new class of near-pan-neutralizing, plasma deconvoluted CD4bs Abs that we refer to as the N49P series. The details of the mechanisms of action of this new Ab class pave the way for the next generation of HIV-1 bnAbs that can be used as vaccine components of therapeutics.

IMPORTANCE Binding to target cell CD4 is the first crucial step required for HIV-1 infection. Thus, the CD4-binding site (CD4bs) is one of the most accessible sites for antibodies (Abs). However, due to steric constraints, only a few Abs are capable of targeting this site. Here, we show that the exceptional neutralization breadth and potency of N49P6, a near-pan-neutralizing Ab targeting the CD4bs isolated from the plasma of an HIV-1 "elite neutralizer," patient N49, are due to its signature combination of more typical CD4bs Ab-binding characteristics with unique interactions with the highly conserved gp120 inner domain. In addition, we also present a structural analysis of N49P6 in complex with the BG505 SOSIP trimer to show that N49P6 exhibits remarkable breadth in part by mimicking CD4's quaternary interaction with the neighboring gp120 protomer. In its mode of antigen interaction, N49P6 is unique and represents a new class of CD4bs-specific bnAbs.

KEYWORDS CD4-binding site, HIV, N49P lineage, near-pan-neutralizing, neutralizing antibodies

Citation Tolbert WD, Nguyen DN, Tehrani ZR, Sajadi MM, Pazgier M. 2021. Near-pan-neutralizing, plasma deconvoluted antibody N49P6 mimics host receptor CD4 in its quaternary interactions with the HIV-1 envelope trimer. mBio 12:e01274-21. https://doi.org/10.1128/mBio.01274-21.

Invited Editor Ivan Dorso, University of Texas Southwestern Medical Center—Dallas

Editor Vanessa Sperandio, University of Texas Southwestern Medical Center—Dallas

Address correspondence to Mohammad M. Sajadi, msajadi@ihv.umaryland.edu, or Marzena Pazgier, marzena.pazgier@usuhs.edu.

Received 30 April 2021
Accepted 15 June 2021
Published 20 July 2021

Broadly neutralization antibodies (bnAbs) capable of neutralizing diverse circulating HIV-1 strains are considered the key for a successful vaccine or passive prophylaxis against HIV-1. High mutation rates, polymorphisms, altered glycosylation patterns forming a protective "glycan shield," and conformational heterogeneity of the envelope glycoprotein (Env) trimer all contribute to HIV-1 variability both within a patient and, to a greater extent, within a population driving viral escape from the immune system (1). Despite these obstacles, potent bnAbs have been isolated that target various distinct vulnerable epitopes within Env, including the CD4-binding site (CD4bs) (2), the V1/V2 loop, the V3 glycan patch (3), the membrane-proximal external region (MPER) (4), and the gp120-gp41 interface (5). Of particular interest is the CD4bs because the infectivity of HIV-1 largely relies on the successful engagement of Env with the host CD4 receptor. Due to this critical functional constraint, conservation of the CD4bs remains relatively high among circulating viruses, rendering them susceptible to neutralizing antibodies. Indeed, members of a group of antibodies targeting CD4bs exhibit both cross-clade neutralization and good potency. Many of them share similar characteristics in heavy chain gene usage and gp120 recognition mode and thus have been categorized as "VRC01 class" antibodies, after the first isolated member (6). The bnAbs within this class typically take longer to develop in natural infection than other bnAb specificities and contain, on average, a high degree of somatic hypermutation (SHM) and a short 5-residue CDR L3 (complementarity-determining region light chain 3) (7, 8). The emergence of single B cell sorting and monoclonal antibody (mAb) isolation enabled the discovery of many potent VRC01 class bnAbs from HIV-infected donors. Of note, some of the most potent CD4bs bnAbs isolated from B cells included N6, 1-18, 3BNC117, and VRC07 (9–12). However, memory B cell repertoires have been shown to differ from those from circulating plasma (13, 14), and there is often a discordance between memory B cell pools and anti-Env circulating antibody responses, which shows that the HIV neutralization profiles of memory B cell-derived mAbs do not always match those found in plasma (15–17).

Recently, by using proteomic and genomic analyses, we described a panel of near-pan-neutralizing antibodies, including N49P7, from the plasma of an HIV-1 "elite neutralizer," donor N49. In addition to being an elite neutralizer, donor N49 belonged to a cohort of viremic controllers within a natural viral suppressor (NVS) cohort of HIV subtype B-infected donors (18, 19). N49P7 was distinct from other bnAbs in the VRC01 class as it made substantially more contact with conserved residues within the gp120 inner domain, contributing to its near-pan-neutralizing ability, with a median 50% inhibitory concentration (IC_{50}) of 0.10 μg/ml (20). Also isolated from donor N49, mAb N49P6 exhibits slightly less potency with a similar remarkable neutralization breadth. A unique feature of both bnAbs N49P6 and N49P7 is that they completely recapitulate the neutralization breadth of the donor N49 anti-Env polyclonal plasma IgG, exhibiting broad and high potency with the ability to neutralize all 117 pseudoviruses in an HIV "global panel." In this study, we characterize the unique mechanisms of the neutralizing activity of bnAb N49P6 by describing the molecular details of N49P6's interaction with monomeric and trimeric Env antigens. The antigen-binding features of N49P6 are discussed in the broad context of antigen recognition of known CD4bs-specific bnAbs, including the VRC01-like class bnAbs, to describe the unique characteristics of Abs of the N49 lineage that allow them to achieve high potency and near-pan-neutralization breadth.

RESULTS

N49P6 shows extraordinary neutralization potency and breadth. Using a multiclade, 117-global-pseudovirus panel, we examined the neutralization activity of monoclonal antibody (mAb) N49P6. Figure 1 shows the neutralization profile of N49P6 compared to N49P7, a near-pan-neutralizing mAb of the same lineage isolated from donor N49 and previously characterized by us (20). N49P6 showed high potency, with a median 50% inhibitory concentration (IC_{50}) and 80% inhibitory concentration (IC_{80}) of 0.31 μg/ml and 0.71 μg/ml,

A

Virus ID	Clade*	IC_{50} (μg/ml)		IC_{80} (μg/ml)	
		N49P6	N49P7	N49P6	N49P7
6535.3	B	0.42	0.19	1.34	0.60
QH0692.42	B	0.65	0.66	2.28	2.41
SC422661.8	B	0.13	0.11	0.36	0.32
PVO.4	B	0.13	0.11	0.36	0.37
TRO.11	B	0.06	0.04	0.19	0.16
AC10.0.29	B	32.31	5.03	>50	36.66
RHPA4259.7	B	0.12	0.08	0.44	0.25
THRO4156.18	B	12.49	2.34	38.40	12.41
REJO4541.67	B	0.07	0.02	0.22	0.05
TRJO4551.58	B	0.26	0.10	0.87	0.35
WITO4160.33	B	0.10	0.08	0.28	0.25
CAAN5342.A2	B	0.66	0.41	1.83	1.21
WEAU_d15_410_787	B (T/F)	0.07	0.05	0.19	0.12
1006_11_C3_1601	B (T/F)	0.07	0.04	0.21	0.16
1054_07_TC4_1499	B (T/F)	0.62	0.49	2.85	2.31
1056_10_TA11_1826	B (T/F)	0.21	0.14	0.61	0.47
1012_11_TC21_3257	B (T/F)	0.14	0.05	0.50	0.13
6240_08_TA5_4622	B (T/F)	0.57	0.46	1.76	1.73
6244_13_B5_4576	B (T/F)	0.10	0.11	0.33	0.39
62357_14_D3_4589	B (T/F)	0.10	0.03	0.30	0.10
SC05_8C11_2344	B (T/F)	0.27	0.16	0.91	0.40
Du156.12	C	0.08	0.03	0.28	0.09
Du172.17	C	20.76	0.10	>50	0.67
Du422.1	C	44.01	4.50	>50	19.55
ZM197M.PB7	C	3.00	0.11	12.40	0.35
ZM214M.PL15	C	0.51	0.21	1.80	0.95
ZM233M.PB6	C	1.23	0.23	4.01	0.77
ZM249M.PL1	C	0.11	0.04	0.38	0.13
ZM53M.PB12	C	0.54	0.25	1.71	0.80
ZM109F.PB4	C	0.08	0.03	0.29	0.15
ZM135M.PL10a	C	0.49	0.20	1.78	0.96
CAP45.2.00.G3	C	21.66	0.06	>50	0.29
CAP210.2.00.E8	C	22.58	1.82	>50	6.49
HIV-001428-2.42	C	0.02	0.01	0.05	0.02
HIV-0013095-2.11	C	0.97	0.07	8.04	0.25
HIV-16055-2.3	C	0.12	0.06	0.59	0.28
HIV-16845-2.22	C	0.69	0.95	3.75	3.94
Ce1086_B2	C (T/F)	0.58	0.09	4.09	0.57
Ce0393_C3	C (T/F)	0.61	0.20	3.25	0.80
Ce1176_A3	C (T/F)	0.59	0.20	2.11	0.59
Ce2010_F5	C (T/F)	0.12	0.13	0.75	0.55
Ce0682_E4	C (T/F)	0.10	0.04	0.32	0.13
Ce1172_H1	C (T/F)	14.35	8.50	47.25	37.52
Ce2060_G9	C (T/F)	0.89	0.66	4.81	2.55
Ce703010054_2A2	C (T/F)	0.25	0.13	0.84	0.47
BF1266.431a	C (T/F)	0.08	0.06	0.28	0.20
246F C1G	C (T/F)	0.51	0.09	2.51	0.26
249M B10	C (T/F)	0.12	0.08	0.55	0.38
ZM247v1(Rev-)	C (T/F)	0.06	0.06	0.17	0.21
7030102001E5(Rev-)	C (T/F)	0.35	0.18	1.17	0.83
1394C9G1(Rev-)	C (T/F)	17.50	3.84	>50	21.07
Ce704809221_1B3	C (T/F)	1.67	0.14	12.77	0.93
CNE19	BC	0.04	0.01	0.16	0.04
CNE20	BC	2.74	0.03	15.64	0.10
CNE21	BC	0.83	0.76	6.52	6.02
CNE17	BC	0.34	0.13	2.10	0.46
CNE30	BC	0.46	0.18	1.54	0.61
CNE52	BC	0.03	0.01	0.10	0.02
CNE53	BC	0.25	0.04	0.87	0.12
CNE58	BC	0.04	0.03	0.10	0.07

Virus ID	Clade*	IC_{50} (μg/ml)		IC_{80} (μg/ml)	
		N49P6	N49P7	N49P6	N49P7
MS208.A1	A	0.11	0.12	0.44	0.48
Q23.17	A	0.05	0.05	0.19	0.21
Q461.e2	A	0.17	0.26	0.62	0.92
Q769.d22	A	0.07	0.03	0.32	0.11
Q259.d2.17	A	24.38	0.33	>50	2.47
Q842.d12	A	0.03	0.02	0.09	0.06
3415.v1.c1	A	0.19	0.16	0.65	0.55
3365.v2.c2	A	0.13	0.07	0.35	0.19
0260.v5.c36	A	0.49	0.35	1.55	0.88
BG505/T332N	A	0.02	0.05	0.08	0.20
191955_A11	A (T/F)	0.12	1.81	0.34	8.87
191084 B7-19	A (T/F)	0.06	0.05	0.26	0.14
9004SS_A3_4	A (T/F)	0.18	0.13	0.82	0.39
T257-31	CRF02_AG	0.15	0.16	0.54	0.62
928-28	CRF02_AG	1.24	0.17	5.60	0.58
263-8	CRF02_AG	0.12	0.06	0.44	0.20
T250-4	CRF02_AG	21.93	2.07	>50	21.42
T251-18	CRF02_AG	0.34	0.18	0.93	0.62
T278-50	CRF02_AG	25.69	22.27	>50	>50
T255-34	CRF02_AG	0.08	0.05	0.39	0.26
211-9	CRF02_AG	8.49	0.22	27.68	0.77
235-47	CRF02_AG	12.98	0.05	46.43	0.30
620345.c01	CRF01_AE	22.90	23.17	>50	47.94
CNE8	CRF01_AE	0.07	0.04	0.25	0.13
C1080.c03	CRF01_AE	0.18	0.11	0.66	0.77
R2184.c04	CRF01_AE	0.03	0.01	0.08	0.03
R1166.c01	CRF01_AE	0.10	0.09	0.34	0.31
R3265.c06	CRF01_AE	0.10	0.05	0.44	0.28
C2101.c01	CRF01_AE	0.14	0.06	0.60	0.34
C3347.c11	CRF01_AE	0.08	0.02	0.27	0.07
C4118.c09	CRF01_AE	0.09	0.04	0.24	0.15
BJOX009000.02.4	CRF01_AE	0.32	0.11	1.46	0.51
BJOX015000.11.5	CRF01_AE (T/F)	0.07	0.04	0.31	0.16
BJOX010000.06.2	CRF01_AE (T/F)	0.68	0.09	3.53	0.59
BJOX025000.01.1	CRF01_AE (T/F)	14.95	0.04	>50	0.24
BJOX028000.10.3	CRF01_AE (T/F)	6.68	0.02	>50	0.12
X1193_c1	G	0.07	0.02	0.22	0.06
P0402_c2_11	G	3.54	0.01	18.95	0.06
X1254_c3	G	15.74	2.97	34.23	13.59
X2088_c9	G	27.04	0.12	>50	0.34
X2131_C1_B5	G	0.17	0.08	0.72	0.27
P1981_C5_3	G	0.31	0.11	0.71	0.27
X1632_S2_B10	G	23.06	12.05	>50	40.38
3016.v5.c45	D	21.67	0.22	>50	1.04
A07412M1.vrc12	D	0.23	0.11	0.79	0.65
231965.c01	D	9.25	0.05	39.39	0.19
231966.c02	D	0.34	0.10	1.62	0.43
3817.v2.c59	CD	16.92	0.72	>50	3.73
6480.v4.c25	CD	0.09	0.03	0.43	0.11
6952.v1.c20	CD	16.91	18.39	>50	38.90
6811.v7.c18	CD	0.24	0.23	1.01	0.99
89-F1_2_25	CD	33.64	21.63	>50	>50
3301.v1.c24	AC	0.05	0.03	0.15	0.07
6041.v3.c23	AC	5.53	0.05	43.15	0.22
6540.v4.c1	AC	13.97	11.75	47.54	33.17
6545.v4.c1	AC	24.49	2.00	>50	14.66
0815.v3.c3	ACD	0.19	0.02	1.25	0.05
3103.v3.c10	ACD	0.58	0.16	1.57	0.51
MuLV	Neg. Control	>50	>50	>50	>50

* (T/F): Transmitted / Founder Virus

B

Clade	Geometric Mean IC_{50} (μg/ml)		Geometric Mean IC_{80} (μg/ml)	
	N49P6	N49P7	N49P6	N49P7
A	0.16	0.09	0.32	0.35
A(T/F)	0.11	0.22	0.42	0.79
B	0.39	0.20	0.83	0.71
B (T/F)	0.17	0.10	0.56	0.34
C	0.91	0.14	1.18	0.54
C (T/F)	0.49	0.20	1.66	0.83
G	2.02	0.19	2.37	0.65
D	1.99	0.11	3.69	0.49
AC	3.18	0.41	6.74	1.65
ACD	0.34	0.05	1.40	0.16
CRF01_AE	0.18	0.09	0.36	0.34
CRF01_AE (T/F)	1.48	0.04	1.05	0.23
CRF02_AG	1.48	0.26	2.50	0.70
BC	0.21	0.05	0.90	0.18
Whole panel	0.54	0.15	0.99	0.52

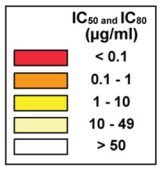

FIG 1 Neutralization profiles of mAbs N49P6 and N49P7. (A) A multiclade, 117-HIV-1-pseudovirus panel was tested against mAbs N49P6 and N49P7. IC_{50} and IC_{80} values are color-coded according to their potencies. Both mAbs N49P6 and N49P7 exhibited 100% breadth, with all pseudoviruses having an IC_{50} of <50 μg/ml. (B) Geometric mean IC_{50} and IC_{80} values of mAbs N49P6 and N49P7 against each clade and the whole panel.

respectively. N49P6, similar to N49P7, exhibits extraordinary neutralizing activity, capable of neutralizing 71.8% of all viruses at an IC_{50} of <1 μg/ml and 49.6% of all viruses at an IC_{80} of <1 μg/ml, compared to 86.3% and 77.8% for N49P7, respectively. Of note, both are among the broadest mAbs discovered thus far and show greater combined breadth and potency than VRC01, VRC07, 3BNC117, NIH45-46, PG9, PG16, PGDM1400, PGT121, PGT128, PGT145, PGT151, 8ANC195, and 10-1074 (20).

N49P6 recognizes highly conserved residues within gp120$_{93TH057}$core$_e$. In order to better understand the features of N49P6 that give it its extraordinary breadth and potency, we determined the crystal structure of N49P6 Fab-gp120$_{93TH057}$core$_e$ to a 2.55-Å resolution (Table 1). As shown in Fig. 2, N49P6 primarily binds through its V_H1-2 heavy chain by mimicking many of the gp120-binding characteristics of CD4. Heavy chain CDR H2 and CDR H3 contribute the most to binding, representing 39% and 27% of the total buried surface area (BSA) of the Fab, respectively (see Table S1 in the supplemental material). CDR H1, in contrast, contributes only 5 Å^2 (0.7%) to the heavy chain BSA. Of these two major anchoring elements, CDR H2 contributes the most to

TABLE 1 Data collection and refinement statistics[a]

Parameter	Value(s) for N49P6 Fab in complex with:	
	HIV-1 clade A/E strain 93TH057 gp120core	HIV-1 BG505 SOSIP.664 Env trimer ectodomain
Data collection		
Wavelength (Å)	0.979	0.979
Space group	$P2_12_12_1$	$P2_13$
Cell parameters		
a, *b*, *c* (Å)	65.4, 80.8, 195.2	164.7, 164.7, 164.7
α, β, γ (°)	90, 90, 90	90, 90, 90
Complexes (ASU)	1	1
Resolution (Å)	50–2.55 (2.59–2.55)	50–4.05 (4.12–4.05)
No. of reflections		
Total	111,144	68,987
Unique	31,853 (1,524)	12,543 (608)
R_{merge}[b] (%)	27.6 (72.7)	11.3 (100)
R_{pim}[c] (%)	16.6 (55.6)	5.3 (75.7)
$CC_{1/2}$[d]	0.99 (0.56)	0.99 (0.48)
Wilson B_{factor} ($1/Å^2$)[e]	41	176
I/σ	6.4 (1.1)	22.8 (1.0)
Completeness (%)	92.0 (89.3)	99.6 (99.8)
Redundancy	3.1 (2.2)	5.5 (4.6)
Refinement statistics		
Resolution (Å)	50.0–2.55	50.0–4.05
R (%)	21.9	25.5
R_{free} (%)	27.3	31.5
No. of atoms		
Protein	5,872	7,725
Water	39	
Ligand/ion	154	544
Overall *B* value ($Å^2$)		
Protein	63	219
Water	55	
Ligand/ion	90	322
Root mean square deviation		
Bond lengths (Å)	0.011	0.008
Bond angles (°)	1.3	1.2
Ramachandran plot (%)		
Favored	91.4	81.2
Allowed	6.5	13.1
Outliers	2.1	5.7
PDB accession no.	6OZ2	6OZ4

[a]Values in parentheses are for the highest-resolution shell. ASU, asymmetric unit.
[b]$R_{merge} = \sum|I - \langle I\rangle|/\sum I$, where *I* is the observed intensity and $\langle I\rangle$ is the average intensity obtained from multiple observations of symmetry-related reflections after rejections.
[c]R_{pim} as defined in reference 53.
[d]$CC_{1/2}$ as defined by Karplus and Diederichs (54).
[e]Wilson B_{factor} as calculated in reference 55.

the BSA of the interface (373 $Å^2$ of the total 733-$Å^2$ heavy chain BSA), which includes a short antiparallel β-sheet (N49P6 residues 55 to 57) that interacts with residues in the gp120 CD4-binding loop (gp120 residues 365 to 368) (Fig. 2B). These contacts are "chaperoned" by a salt bridge between Asp^{368} of gp120 and a heavy chain framework region 3 (FWR3) residue of N49P6, Arg^{71}, found in many VRC01-like bnAbs (Fig. 2C). In addition, CDR H2 also interacts with gp120 loop D (through a hydrogen [H] bond formed between Trp^{50} [CDR H2] and Asn^{280} [loop D]) and gp120 loop V5 (through contacts with gp120 residues 455 to 459). Interestingly, although N49P6 mimics many of CD4's binding characteristics, Gly^{54} in CDR H2 of N49P6 bypasses the Phe^{43} (CD4)-binding cavity, a hydrophobic pocket used by CD4 and many CD4 mimetics to bind to Env (Fig. 2B). N49P6 shares this feature with N49P7, which indicates that this Ab lineage

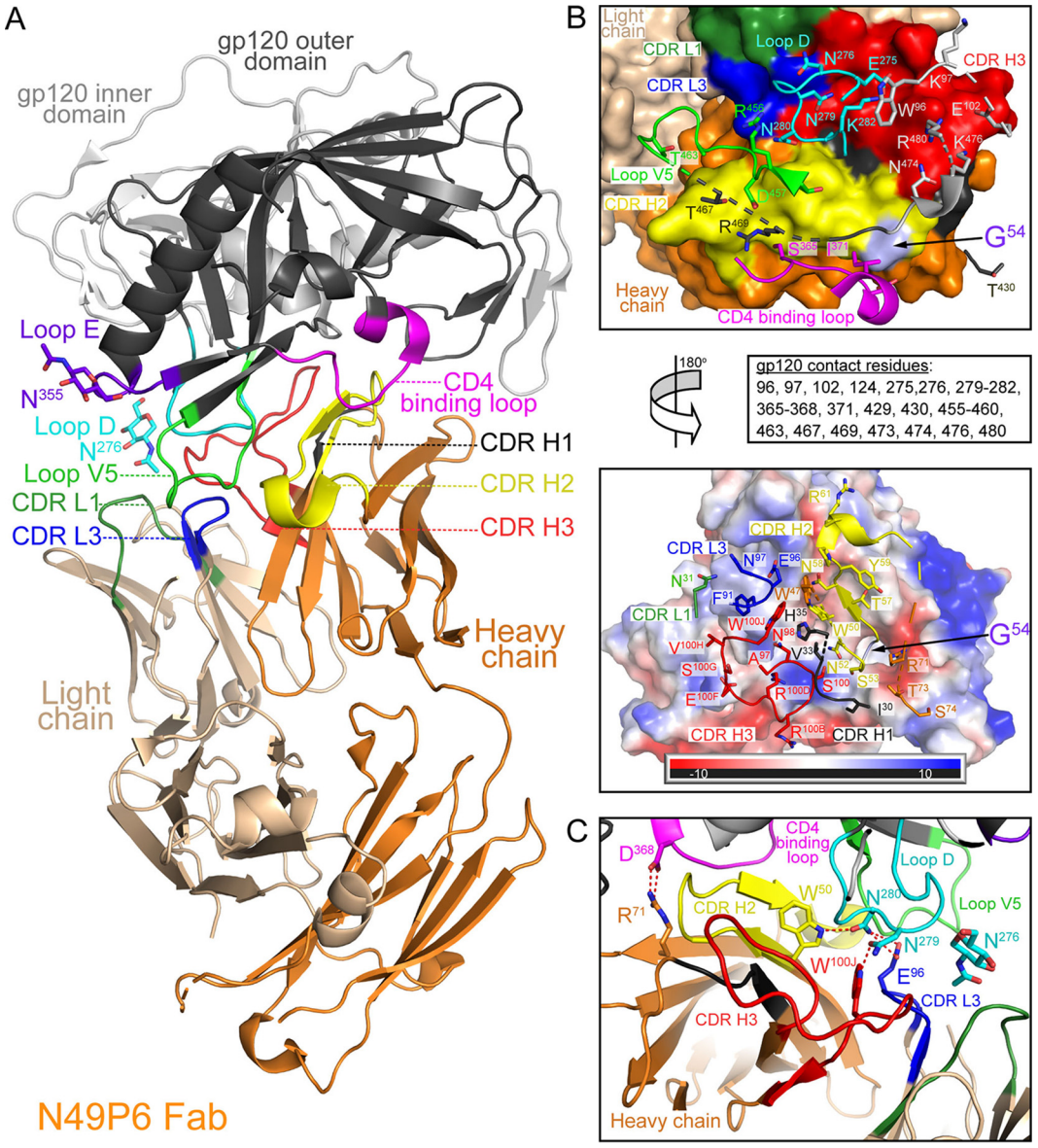

FIG 2 Crystal structure of the N49P6 Fab-gp120$_{93TH057}$core$_e$ complex. (A) Overall structure of the complex shown as a ribbon diagram. The complementarity-determining regions (CDRs) of N49P6 Fab are colored as follows: CDR H1 is black, CDR H2 is yellow, CDR H3 is red, CDR L1 is dark green, and CDR L3 is blue. The outer and inner domains of gp120 are dark and light gray, respectively. The outer domain D and E, CD4 binding, and V5 loops are shown in cyan, purple-blue, magenta, and green, respectively. Carbohydrates at positions N^{276} (loop D) and N^{355} (loop E) are shown as sticks. (B) N49P6 Fab-gp120$_{93TH057}$core$_e$ interface with coloring as described above for panel A. (Top) N49P6 Fab is shown as a molecular surface, and the gp120 contact residues are shown as sticks. (Bottom) A 180° view reveals the detailed interaction of N49P6 Fab and the gp120 surface. Contact residues of N49P6 Fab are shown as sticks, and all Fab contact residues are listed. gp120 is shown as a molecular surface and colored according to its electrostatic potential, with red, blue, and white representing negative, positive, and neutral electrostatic potentials, respectively. (C) Blowup view of the hydrogen bond network of the interaction between N49P6 Fab and the gp120 surface. Three hydrogen bonds (CDR H2 W^{50} and loop D N^{280}, CDR H3 W^{100J} and loop D N^{279}, and CDR L3 E^{96} and loop D N^{280}) and a salt bridge (heavy chain residue R^{71} and CD4-binding loop D^{368}) are formed at the interface. Residues contributing to the interaction are shown as sticks, and the hydrogen bond network is shown with red dashed lines.

developed an alternate strategy to compensate for the loss of binding energy by using Gly instead of an amino acid with a bulky hydrophobic side chain at this position (20); some, but not all, VRC01-like Abs use the Phe^{43} cavity for binding Env, although this may decrease the breadth in the presence of cavity-filling mutations such as Ile^{375} in the N6-resistant pseudovirus CT565_C7_48. An important anchoring element that may

compensate for this loss in N49P6 is the 20-amino-acid (aa)-long CDR H3 (Fig. 2B and C). N49P6's CDR H3 contacts gp120 loop D (gp120 residues 275 to 276 and 279 to 283), establishing a Trp^{100J} (CDR H3)-Asp^{279} (loop D) hydrogen bond, and contacts the conserved gp120 inner domain layer 3 (gp120 residues 474 and 476). As we discuss below, the inner domain contacts are unique to the N49 lineage.

The contribution of the N49P6 lambda light chain to the gp120 core complex interface is minimal, representing only 25% of the total Fab BSA (18% if excluding the contribution from the Asn^{278} glycan). N49P6's light chain contains both deletions in its 8-amino-acid-long CDR L1 and a shortened CDR L3 to minimize light chain-mediated viral escape. The truncated CDR L1 contacts only the *N*-acetylglucosamine linked to Asn^{276} on gp120 loop D. The short CDR L3 also contacts the Asn^{276} glycan as well as neighboring residues in loop D (gp120 residues 276 and 278 to 280) and loop V5 (gp120 residues 458 to 459), with CDR L3 Phe^{91} making van der Waals contacts with gp120 Asn^{279} and Thr^{278} and CDR L3 Glu^{96} forming a hydrogen bond with the gp120 Gly^{459} main chain. Steric clashes between the light chain and the Asn^{276} glycan are a major limiting factor in breadth for CD4bs bnAbs, with most having deletions in CDR L1 in addition to a 5-residue CDR L3; N49P6 has one of the shortest CDR L1s, 1 amino acid shorter than VRC01 and 3 amino acids shorter than N6 (Fig. S1). In addition, N49P6 and N49P7 have a Cys at framework residue 36 of the light chain, normally Tyr, which allows the light chain to rotate further away from gp120 and better accommodate the Asn^{276} glycan (20).

N49P6 closely resembles N49P7 in binding to $gp120_{93TH057}core_e$. N49P6 is clonally related to N49P7, another antibody from the same donor. N49P6 and N49P7 share similar breadths, with N49P7 being slightly more potent (Fig. 1). The available high-resolution crystal structure of the complex of the N49P7 Fab with $gp120core_e$ of the same clade A/E 93TH057 strain determined by us previously (20) allowed us to compare their mechanisms of attachment and determine what contributes to the breadth and potency of this antibody class. Figure 3 shows a structural comparison of both complexes and a detailed analysis of specific antibody-antigen contacts. Superimposition of the N49P6 and N49P7 complexes based upon $gp120_{93TH057}core_e$ (Fig. 3A) revealed no significant structural differences (C_α carbon root mean square deviations of 1.53 Å for the complex and 0.89 Å for the complex minus the constant part of the Fab), although N49P6 has a 1-amino-acid-longer CDR H3 than N49P7 (Arg^{100C} represents an insertion in N49P6 relative to N49P7). In the N49P6 gp120 complex, Arg^{100C} points away from gp120 and does not contribute to binding. However, we noticed a slight difference in the relative orientations of V_L and V_H in the N49P6 structure, with V_L tilting further away from loop D, which results in a slightly smaller light chain footprint on gp120, as shown in Fig. 3B. Both N49P6 and N49P7 recognize a mixed inner domain/CD4-binding-site epitope referred to as the iCD4bs epitope, which is composed of highly conserved regions in gp120 (Fig. 3D). As shown in other studies, the gp120 inner domain, consisting of three mobile layers and a 7- or 8-stranded β-sandwich, contributes to Env integrity as well as to conformational transitions during viral fusion and therefore harbors some of its most highly conserved residues (21, 22). Specifically, CDR H2 and CDR H3 of N49P6 interact with residues 97, 102, and 124 of layer 2 and residues 473, 474, 476, and 480 of layer 3.

Interestingly, structural analyses indicate that the slightly lower neutralization potency of N49P6 than of N49P7 can be attributed to a few sequence changes in CDR H2 and CDR H3 (lower BSA due to Ser^{53}-versus-Met, Gly^{56}-versus-Gln, and Thr^{57}-versus-Val differences). In addition, the insertion of an extra Arg in CDR H3 of N49P6 (Arg^{100C}) relative to N49P7 results in a slightly lower BSA for Glu^{100F} and Val^{100H}, even though their side chain positions are largely superimposable (Fig. 3C and D). The only other significant difference in BSAs between the two epitopes resides on the light chain, with N49P7 having a slightly higher BSA in its CDR L3 due to a Phe^{91}-versus-Tyr difference in their sequences.

N49P6 and N49P7 are unique among VRC01-like CD4bs Abs in how they extend their gp120 footprint and increase their neutralization breadth. The CD4-binding site is recessed in the HIV-1 trimer and provides only limited access to binding partners. Only a few classes of Abs that target this site can meet these requirements and effectively neutralize HIV-1, i.e., those derived from the heavy chain germ line allele V_H1-2 (VRC01 class) or V_H1-46 (8ANC131 class) and those that predominately bind with their

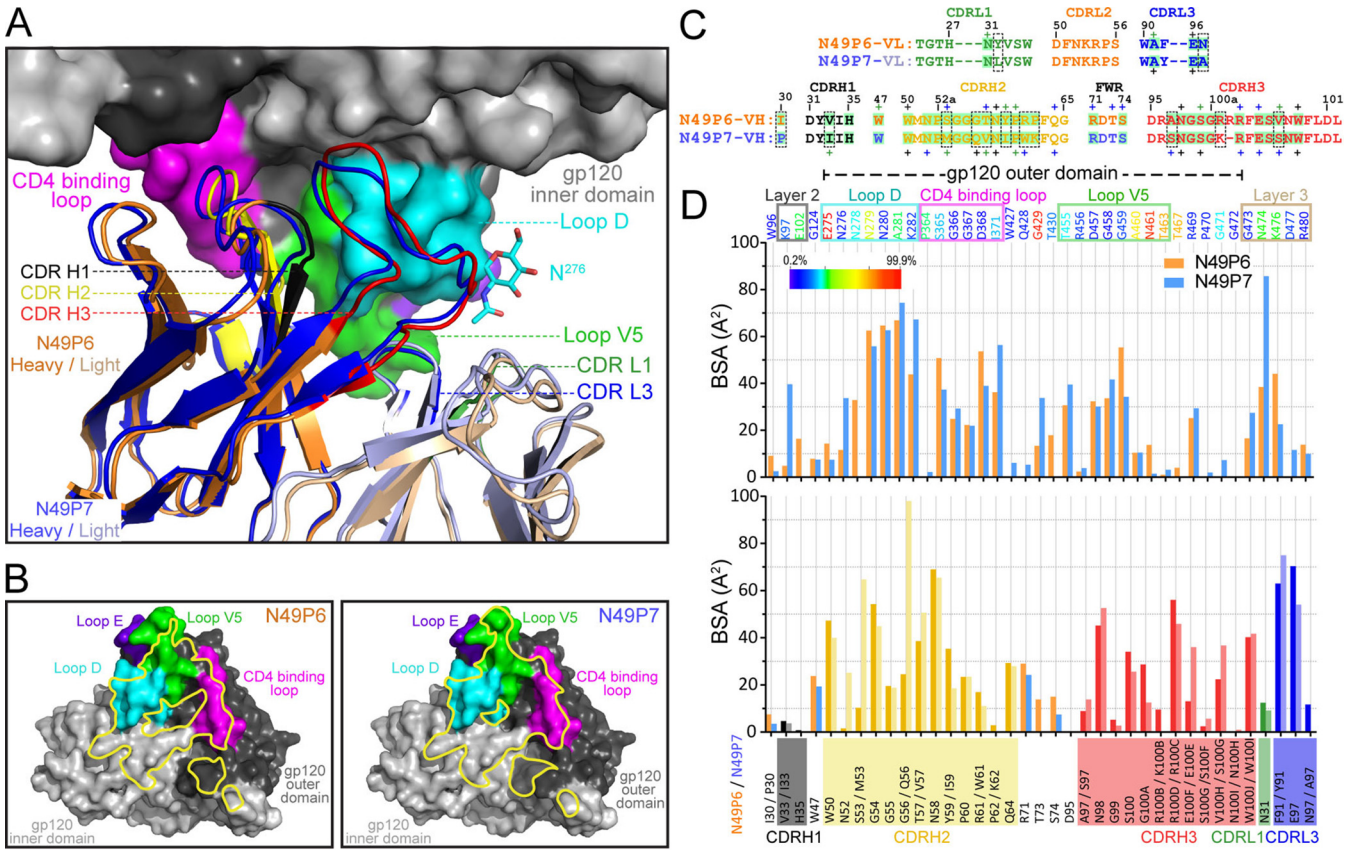

FIG 3 Structural comparisons of N49P6 Fab- and N49P7-gp120$_{93TH057}$core$_e$ complexes. (A) Blowup view into the Fab-gp120core$_e$ interface. The molecular surface is displayed over gp120$_{93TH057}$core$_e$, and the CDRs of N49P6 are shown as sticks, with colors as described in the Fig. 2 legend. The heavy chain and light chain of N49P7 are shown in dark and light blue, respectively. All structures were superimposed based on gp120$_{93TH057}$core$_e$. The N49P7 Fab-gp120$_{93TH057}$core$_e$ structure is from PDB accession number 6BCK. (B) Binding footprints for N49P6 and N49P7 on gp120$_{93TH057}$core$_e$ are outlined in yellow. The gp120 surface is colored as described in the Fig. 2 legend. (C) Contact residues of CDRs of N49P6 and N49P7 with gp120$_{93TH057}$core are mapped onto the primary sequences. Contact residues are defined by a 5-Å cutoff and marked above the sequence with + for the side chain and − for the main chain to indicate the type of contact. Contact types are colored as follows: green for hydrophilic, blue for hydrophobic, and black for both. Buried surface residues were determined by PISA and are shaded in green. Residues that differ between N49P6 and N49P7 are highlighted with dashed boxes. (D) Buried surface area (BSA) contributions to binding of gp120 residues (top) and N49P6/N49P7 Fab residues (bottom) as calculated by PISA. (Top) The gp120 sequence is color-coded in a gradient based on its sequence conservation: dark blue corresponds to the percentage of sequences in the HIV sequence compendium (https://www.hiv.lanl.gov/content/sequence/HIV/COMPENDIUM/compendium.html) that differ at that position from the Hxbc2 reference sequence 0.2 to 7% of the time, and red corresponds those that differ at that position from Hxbc2 87 to 99.9% of the time. Intermediate colors correspond to intermediate percentages on a roughly linear scale. Inner domain layers 2 and 3 and the outer domain D, V5, and CD4-binding loops are colored as described in the legend of Fig. 2. BSA contributions for N49P6 and N49P7 contact residues are shown. (Bottom) CDRs H1, H2, H3, L1, and L3 are colored as described in the legend of Fig. 2. BSA contributions to binding for N49P6 and N49P7 CDR residues are shown in darker and lighter shades of the CDR color, respectively, and those for FWR residues shown in orange and blue, respectively.

CDR H3 (6). To better understand how N49P6 and also N49P7 fit into these categories, we compared their structures to those of bnAbs of this class whose gp120core structures are available, specifically, VRC01, VRC03, VRC07, NIH45-46, and N6 (Fig. 4 and Fig. S1). As can be expected due to their shared germ line V_H1-2 allele, there is a high degree of similarity in how CDR H2 of each of these Abs binds gp120. The Thr^{57}-to-Val difference between N49P6 and N49P7 that results in an approximately 12-Å^2 increase in the BSA for N49P7 seems common for all other members examined here (Fig. S1); Thr^{57} in N49P6 forms a weak hydrogen bond with gp120 Gly^{366} and may not pack as well against Ser^{365} as does Val^{57} in N49P7, which forms van der Waals contacts with both residues. Similarly, the choice of a larger hydrophobic residue than serine at position 53 seems the norm, with Met for N49P7 and Leu or Arg for all others except N6 with Gln.

A common strategy used by VRC01-like Abs to increase binding energy is the use of the CD4 Phe^{43}-binding cavity. Both VRC03 and N6 do this by having a Trp or Tyr at heavy chain position 54, respectively. N49P6 and N49P7 but also VRC01, VRC07, and NIH45-46 have a

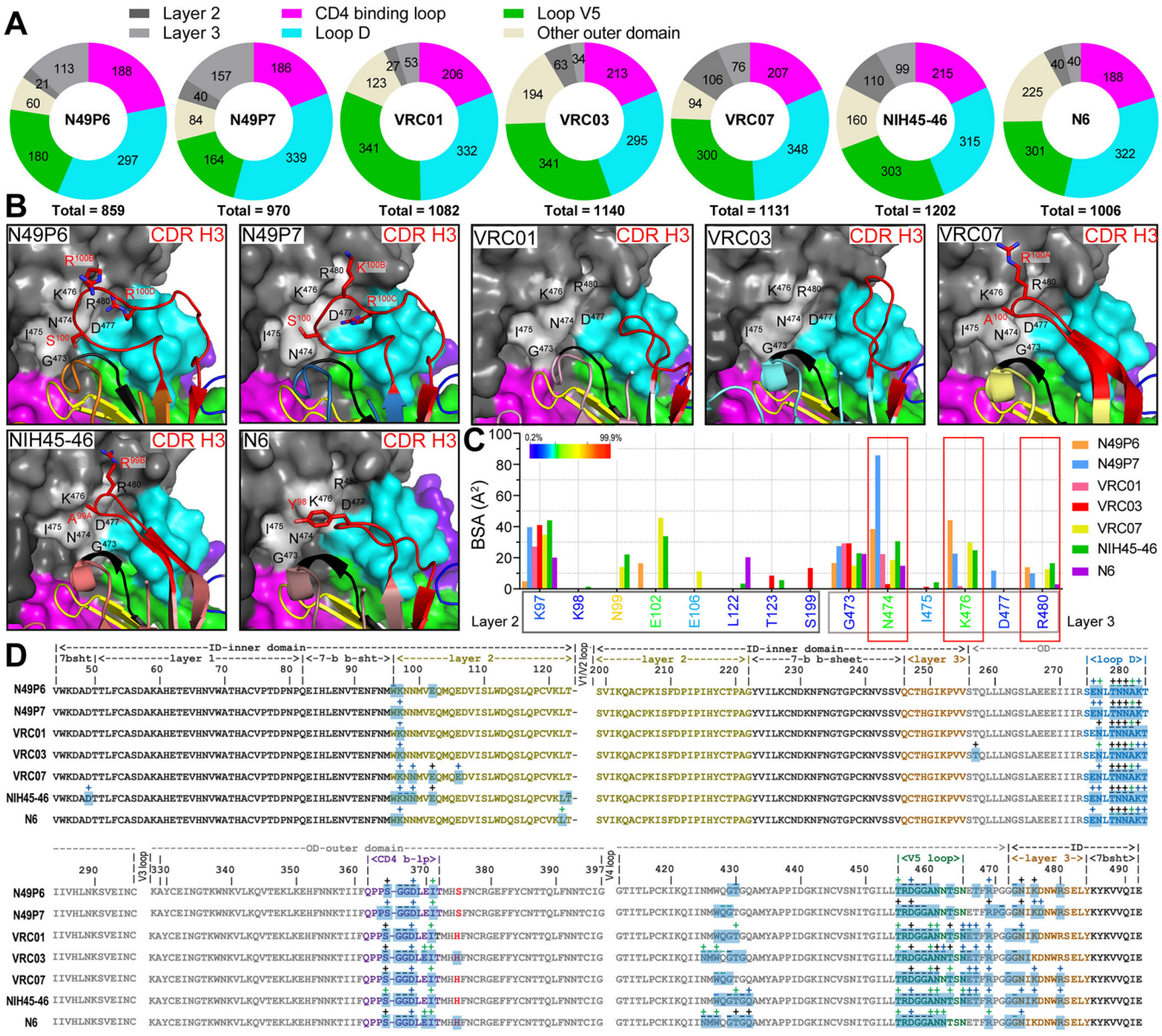

FIG 4 Structural comparison of binding modes between N49P6 and other broadly neutralizing CD4-binding-site antibodies. (A) Pie charts showing the buried surface area (BSA) contributions to gp120 binding. The outer domain loops: D, CD4 binding, and V5 are colored as shown. The other outer domain and layers 2 and 3 of inner domain are also colored as shown. (B) Comparison of interactions between layers 2 and 3 of the gp120 inner domain and CDR H3 of N49P6 with other bnAbs (N49P7, VRC01, VRC03, VRC07, NIH45-46, and N6). The molecular surface is displayed over the gp120core, and the CDRs are shown as a ribbon diagram, with coloring as described in the legend of Fig. 2. Layers 2 and 3 of the gp120 inner domain are shown in darker and lighter shades of gray, respectively. Layer 3-contacting residues are labeled on the surface of gp120. (C) BSA contributions to layer 2 and 3 binding for a range of broadly neutralizing CD4bs antibodies (N49P6, N49P7, VRC01, VRC03, VRC07, NIH45-46, and N6). Residues of layers 2 and 3 are color-coded based on their sequence conservation as described in the legend of Fig. 3. BSA values for N49P6, N49P7, VRC01, VRC03, VRC07, NIH45-46, and N6 contact residues are shown. (D) Contact residues of gp120 mapped onto the $gp120_{93TH057}$core sequences. Contact residues are defined by a 5-Å cutoff and marked above the sequence with + for the side chain and − for the main chain to indicate the type of contact. Buried surface residues were determined by PISA and are shaded blue.

glycine at position 54 and leave this cavity empty (Fig. S1). Phe^{43} cavity-filling mutations such as those found in many clade A/E HIV-1 strains, e.g., His^{375}, may interfere with a bulky side chain at this position, as is seen for many small-molecule CD4-mimetic compounds that rely heavily on the Phe^{43} cavity. Having Gly at position 54 may therefore contribute to increased breadth at the expense of potency, although for CD4bs Abs, this explanation may not be as straightforward since His^{375}, at least in the case of N6, does not prevent binding and neutralization (9).

N49P6 and N49P7 are unique in their use of long 20- and 19-aa CDR H3s, respectively. These are the longest found among VRC01 class Abs; the next longest, found in VRC07 and NIH45-46, have 16-aa CDR H3s (Fig. S1). As shown in Fig. 4, the elongated CDR H3s allow N49P6 and N49P7 to increase their binding footprint to include the gp120 inner domain, specifically gp120 inner domain layer 3. N49P6 and N49P7 have the largest BSA contribution with gp120 inner domain layer 3 to the total BSA of the complex among all VRC01 class Abs (113 and 157 Å^2 for the N49P6 and N49P7 complexes, respectively, compared to a range of 34 to 99 Å^2 for the other CD4bs bnAb complexes) (Fig. 4A). These include contacts with conserved and highly conserved residues at positions 474, 476, and 480 of gp120 layer 3 mediated by Ser^{100}, Lys/Arg^{100B}, and Arg^{100D} of the extended CDR H3 of N49P6/P7 (Fig. 4B and C); VRC07, NIH45-46, and N6 but not VRC01 and VRC03, reach residues in gp120 inner domain layer 3 through CDR H3 contacts mediated by Ala^{100}/Ala^{99A} and Arg^{100A}/Arg^{99B} of VRCO7/NIH45-46 and Tyr^{98} of N6. VRC07 and NIH45-46 also rely on gp120 inner domain layer 2 contacts in an area also recognized by N49P6 and N49P7 but with noticeably lower BSAs. In contrast, the more typical VRC01-like bnAbs, including VRC01, VRC03, and, to a lesser extent, N6, use their CDR H3 to almost contact loop D residues exclusively, with limited contact with the layers in the gp120 inner domain (Fig. 4). The use of the conserved gp120 inner domain residues may be an important component contributing to the breadth of Abs targeting the CD4bs. It is worth noting that VRC07 and NIH45-46 are among the broader and more potent bnAbs in the VRC01-like class. N49P6 and N49P7 neutralize 98/117 (83.8%) and 115/117 (98.3%) members of the 117-pseudovirus panel with IC_{80} values of $<50\,\mu$g/ml and 86/117 (73.5%) and 103/117 (88%) members with IC_{80} values of $<10\,\mu$g/ml, respectively. VRC07 and NIH45-46 neutralize 106/116 (91.4%) and 94/110 (85.5%) members of the panel with IC_{80} values of $<50\,\mu$g/ml and 102/116 (87.9%) and 88/115 (76.5%) members with IC_{80} values of $<10\,\mu$g/ml. To put things into perspective, the MPER bnAb 10E8 neutralizes 88/114 (77.2%) members of the panel with IC_{80} values of $<10\,\mu$g/ml.

N49P6 utilizes interprotomer contacts for binding to the HIV-1 trimer. To further investigate the interaction of N49P6 with HIV-1 Env antigen, we determined the crystal structure of N49P6 Fab in complex with BG505 SOSIP.664 at a 4.05-Å resolution (Table 1). Figure 5A shows the structure of the full complex generated by crystallographic symmetry, which consists of three gp120s, three gp41s, and three N49P6 Fabs. Each CD4bs of the trimer is occupied by an N49P6 Fab, and the primary contact for the Fab is the CD4bs, which largely mirrors the interaction of the Fab and gp120 in the monomer complex structure (Fig. 5B). The total CD4-binding loop BSAs are 188 Å^2 and 184 Å^2 for gp120 and trimer complexes, respectively; the loop D BSAs are 297 Å^2 and 310 Å^2; and the loop V5 BSAs are 180 Å^2 and 240 Å^2 (Table S1). Differences in BSAs for the CD4bs between the monomer and trimer structures can largely be attributed to differences in sequence between clade A/E 93TH057 and clade A BG505 gp120 and differences in conformation due to deletions in the V1/V2 and V3 loops in the gp120 core structure, which can be seen in the BSA plot versus residue positions (Fig. 5C). The difference in sequence in loop V5 (residues 460 and 461) and layer 3 (residues 474 and 476) influences the BSAs for these residues and also likely neighboring residues, i.e., Gly^{459} and Gly^{473}. A major conformational change at Gln^{428} represents the largest single-residue difference in BSAs between the two structures. Gln^{428} sits on the β20-β21 turn on the outer domain half of the bridging sheet, which is formed in the monomer but not the trimer complex. The inner domain half of the bridging sheet, the V1V2 loop, extends to the top of the trimer, which disrupts the bridging sheet in the trimer, while a deletion in the V1V2 loop facilitates its formation in the monomer. The better packing of N49P6 around Gln^{428} in the trimer in the absence of the bridging sheet is likely also an explanation for the slightly higher BSA for the trimer residue E^{102} than for the monomer due to their proximity in the two structures. Conversely, the higher BSA for the monomer in loop D residues around Asn^{276} may reflect differences in the glycans between the two structures. The gp120 complex was made

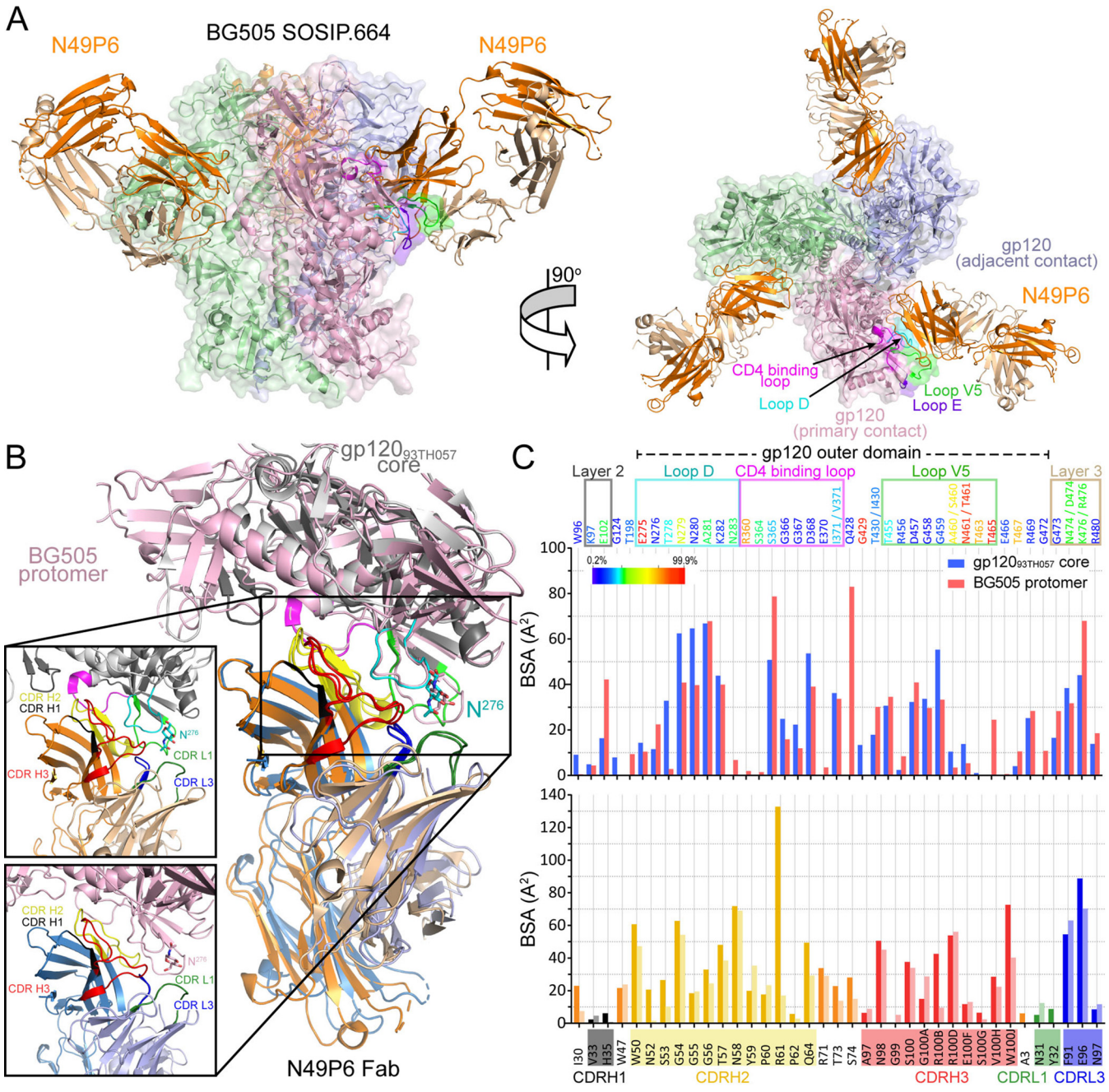

FIG 5 Overall structure of the N49P6 Fab-BG505 SOSIP.664 trimer complex. (A) Side and top views of the crystal structure of a ternary complex of the BG505 SOSIP.664 HIV-1 Env trimer and three N49P6 Fabs (orange) in ribbon representation. Each gp120-gp41 protomer is shown in a different color. The outer domain loops are shown in primary gp120 contact and colored as described in the legend of Fig. 2. (B) Structural comparison of the N49P6 Fab-gp120$_{93TH057}$core$_e$ complex and the N49P6 Fab-gp120 (primary contact) protomer of the BG505 trimer. The complexes are superimposed based on gp120$_{93TH057}$core$_e$. The N49P6 Fab-gp120$_{93TH057}$core$_e$ complex is colored as described in the legend of Fig. 2, and the heavy and light chains of N49P6 Fab in the N49P6-BG505 protomer complex are shown in dark and lighter shades of blue, respectively. The enlargements show the contacts between N49P6 Fab and gp120$_{93TH057}$core (top) and the BG505 protomer (bottom). (C) BSA contributions to binding of gp120 (93TH057 core and BG505 gp120 [primary contact] protomer) residues (top) and N49P6 residues (bottom) as calculated by PISA. (Top) The gp120 sequence is color-coded based on its sequence conservation as described in the legend of Fig. 3. Inner domain layers 2 and 3 and the outer domain D, V5, and CD4-binding loops are colored as described in the legend of Fig. 2. BSA values for N49P6 and N49P7 contact residues are shown in blue and red, respectively. (Bottom) All CDRs, H1, H2, H3, L1, and L3, are colored as described in the legend of Fig. 2. BSA contributions to binding of N49P6 contact residues to gp120$_{93TH057}$core$_e$ and the primary BG505 protomer are shown in darker and lighter shades of the CDR color, respectively.

with HEK 293 GnT1-grown protein with all but the initial *N*-acetylglucosamine removed by Endoglycosidase H (EndoH$_f$) (New England BioLabs). The glycan on Asn^{276} in the trimer structure is present but disordered past the initial *N*-acetylglucosamine; the trimer complex was also made from GnT1-grown protein, but the

high-mannose N-glycans were left intact in the protein used for crystallization. The truncated glycan may permit N49P6 to have a more stable light chain interaction in the monomer than in the trimer, although the total light chain contributions to the BSA are largely identical between the two, 245 Å^2 for the monomer and 258 Å^2 for the trimer; the light chain's contribution to binding is almost exclusively to the glycan at Asn^{276} and nearby residues in both structures.

Although the primary CD4bs for both complexes are similar, contacts with the adjacent protomer increase the BSA of the complex formed by each N49P6 Fab with the trimer to make it significantly larger (Table S1). These interprotomer interactions are identical for each Fab due to crystal symmetry and are made mostly by the framework region immediately preceding CDR H1 and one CDR H1 residue (Gly^{26}, Tyr^{27}, Asp^{28}, and Tyr^{32}). CDR H3 adds two arginines to the interface (Arg^{96} and Arg^{100C}), including the one (Arg^{100C}) inserted in the CDR H3 relative to N49P7 (Fig. 5A and B). Contacts within the adjacent promoter map to mobile layer 1 on the gp120 inner domain and include Tyr^{61}, Glu^{64}, Lys^{65}, and His^{66} with Fab-gp120 hydrogen bonds (the carbonyl oxygen of Gly^{26} [FWR1] and the side chain of Lys^{65}, the side chains of Asp^{28} [FWR1] and His^{66}, the side chains of Tyr^{32} [CDR H1] and Glu^{64}, the side chains of Arg^{96} [CDR H3] and Glu^{64}, and the side chains of Arg^{100C} [CDR H3] and Tyr^{61}) and hydrophobic van der Waals interactions (formed between the side chains of Tyr^{27} [FWR1] and Lys^{65}). The total BSA of the interface is 429 Å^2, 207 Å^2 from the trimer and 222 Å^2 from the heavy chain of N49P6, which adds approximately 15% more BSA to the trimer and 17% more BSA to the Fab (Fig. S1).

N49P6 mimics CD4 in its initial quaternary interaction with BG505 SOSIP.664. It has been shown previously that the first CD4 that binds a BG505 SOSIP trimer has both a primary and a secondary binding site (23). The primary site is essentially identical to that used in CD4 structures with monomeric gp120 (24). The secondary CD4bs resides on the adjacent gp120 within inner domain layer 1 (23). Interestingly, a structural alignment of the complexes formed between the BG505 SOSIP.664 trimer and three N49P6 Fabs or a single CD4 molecule (Protein Data Bank [PDB] accession number 5U1F) (23) reveals that the layer 1 gp120 residues used by N49P6 to contact the adjacent protomer are largely identical to the ones that CD4 uses in its initial quaternary interaction with the trimer (Fig. 6A through C). Although the resolution of the monovalent CD4-BG505 SOSIP.664 trimer complex was low, which introduces some ambiguity into the details of the interface, the CD4 contacts with the adjacent protomer were mapped to residues 62 to 66 of layer 1 and within the coreceptor-binding site, Lys^{207}. (Fig. 6B) (23). Interestingly, N49P6's interprotomer contacts involve three (Glu^{64}, Lys^{65}, and His^{66}) of five residues utilized by CD4 within layer 1. Of note, residues Glu^{64}, His^{66}, and Lys^{207} are almost universally conserved across HIV-1 isolates, and mutational studies confirm their importance in proper spike function and viral infectivity (23). N49P6 capitalizes on the functional importance and the sequence conservation of these residues to increase its affinity and breadth.

It has been shown previously that the one CD4-bound BG505 SOSIP trimer transitions very quickly to a more open conformation with three CD4s bound that fully exposes the coreceptor-binding site (25). In this state, the contacts of CD4 with the adjacent protomer are lost (26) (Fig. 7). The binding of coreceptor or coreceptor-binding-site antibody stabilizes this open conformation with a few additional changes (26, 27). Charge inversion within the quaternary CD4-binding site in HIV-1 Env of His^{66} to Glu or Glu^{62} to Lys and Glu^{64} to Lys abrogates viral infectivity, highlighting the importance of this region (23). It is interesting to note that N49P6 interacts with these residues much like a charge-inverted virus to CD4, with Asp^{28} (N49P6) forming a hydrogen bond to His^{66} of the adjacent gp120 in the trimer and Arg^{96} (N49P6) forming a hydrogen bond to Glu^{64} (gp120) (Fig. 6C). The inferred binding based on distance in the CD4 complex is between Lys^{21} (or Lys^{22}) (CD4) and His^{66} (gp120) and between Gln^{20} (CD4) and Glu^{64} (gp120), which would seem less stabilizing. This may reflect CD4's role in infection, which is to drive the transition to an open conformation and expose the coreceptor-binding

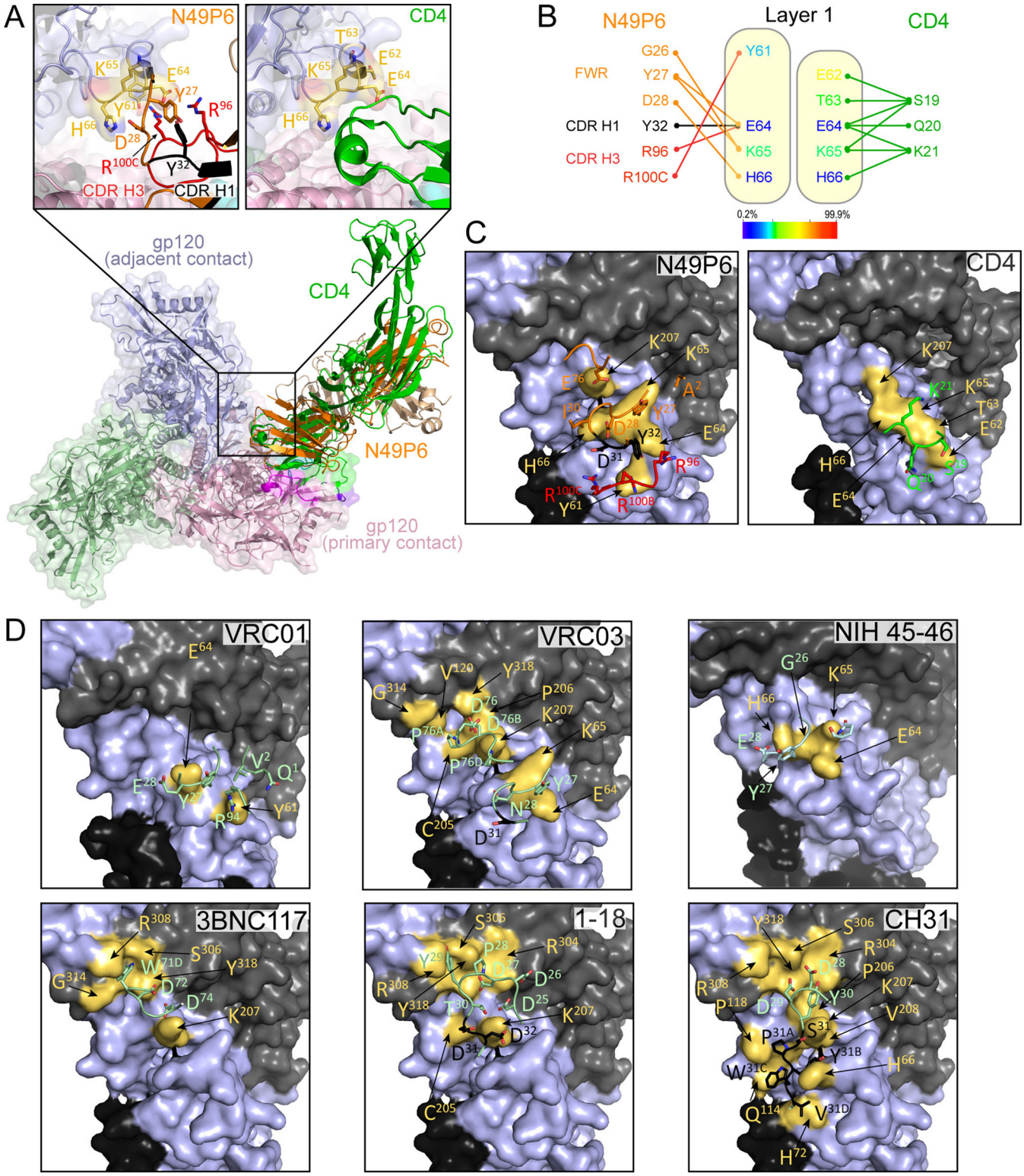

FIG 6 Molecular details of the interprotomer contacts of N49P6. (A) Structural alignment of the N49P6 Fab-BG505 SOSIP.664 trimer complex and the BG505 SOSIP.664 trimer with one CD4 molecule bound (PDB accession number 5U1F). N49P6 Fab (orange) and CD4 (green) are shown as a ribbon diagram. The zoomed-in views depict the contact between N49P6 Fab or CD4 and the adjacent BG505 protomer. All contacting residues are shown as sticks. (B) Networks of interactions formed between N49P6 Fab/CD4 and the adjacent gp120 BG505 protomer as defined by either a 5-Å distance criterion cutoff for N49P6 or a 7.5-Å distance criterion cutoff for CD4 are shown as solid lines. Layer 1 residues are color-coded based on their sequence conservation as described in the legend of Fig. 3. (C) Binding footprints of N49P6 and CD4 on the adjacent gp120 BG505 protomer (surface representation) are colored in yellow. Contacting residues of N49P6 and CD4 are shown in a stick representation (framework region [FWR] in orange, CDR H1 in black, CDR H3 in red, and CD4 in green). (D) Binding footprints of other CD4bs Fabs (VRC01 [PDB accession number 5FYJ], VRC03 [PDB accession number 6CDI],

(Continued on next page)

site. In contrast, N49P6's role in neutralization is to bind and lock the trimer in a closed state.

The N49P6 quaternary interaction is different from the quaternary interactions of other potent CD4bs Abs. N49P6 is not the only CD4bs bnAb to extend its footprint onto the adjacent protomer. Many of the broader and more potent CD4bs bnAbs use different interprotomer contact strategies to lock the trimer in a more closed conformation; some target elements of the gp120 inner domain, while others target the coreceptor-binding site at the base of the V3 loop. Figure 6C and D show the interprotomer contact details of many of these bnAbs compared to N49P6 and CD4. The most like N49P6 is the prototypic VRC01 class Ab VRC01, which binds to inner domain layer 1 of the adjacent gp120 with a total BSA of 102 Å^2, compared to 206 Å^2 for N49P6, 199 Å^2 from layer 1 and 7 Å^2 from layer 2 (2, 28). VRC03, another VRC01 class Ab from the same donor, uses heavy chain framework residues and a unique insertion in the heavy chain framework region to contact gp120 inner domain layer 1, 42 Å^2, but relies more heavily on inner domain layer 2, 90 Å^2, and the base of the V3 loop, 47 Å^2, for a total gp120 BSA of 179 Å^2 (29, 30). NIH45-46 also contacts inner domain layer 1 on the adjacent trimer, 38 Å^2, but without the heavy chain framework insertion contacts only layer 1. 3BNC117 contacts the adjacent gp120 inner domain layer 1, 40 Å^2, and the base of the V3 loop, 125 Å^2, for a total of 165 Å^2 (31). Similarly, CH31 uses both heavy chain framework and CDR H1 residues to bind the adjacent gp120 inner domain layer 1, 100 Å^2; layer 2, 140 Å^2; and the base of the V3 loop, 92 Å^2; for a total of 332 Å^2 (29, 30). And finally, 1-18 uses its heavy chain framework and CDR H1 residues to contact inner domain layer 2, 104 Å^2, and the base of the V3 loop, 175 Å^2, for a total BSA of 279 Å^2 (Table S2) (10).

An important consideration when comparing quaternary contacts in the trimer is the degree to which the trimer "opens" upon Ab binding. The HIV-1 BG505 SOSIP trimer goes from a "closed" trimer with distances between protomers as measured by the α-carbon of residue 375 at the base of the Phe^{43} cavity of 54.5 Å to an average of 69.6 Å in the fully open trimer with three CD4s bound (Fig. 7). The degree to which a trimer opens determines the degree to which quaternary contacts are possible. It is worth noting that all the CD4bs bnAbs that make contacts with the adjacent gp120 have BG505 SOSIP trimers in a more closed conformation, more closed than even the BG505 SOSIP trimer with only one CD4 bound, which has an average distance of 57.4 Å. The average distance between protomers ranges from 54.5 to 55.9 Å, with N49P6 having an average interprotomer distance identical to that of the unbound BG505 SOSIP trimer, 54.5 Å. Some BG505 SOSIP trimers are asymmetric, like NIH45-46, which has quaternary contacts for only two of the three possible adjacent protomers in the trimer, but most are largely symmetric. NIH45-46 also has the smallest adjacent protomer footprint, which may explain its inability to lock its BG505 SOSIP trimer in a closed conformation.

N49P6's total adjacent protomer footprint is larger than those of VRC01, VRC03, NIH45-46, and 3BNC117 but smaller than those of 1-18 and CH31. However, N49P6 has the largest BSA for the inner domain layer 1 region that overlaps CD4's interprotomer footprint, twice the layer 1 footprints of VRC01 and CH31 and roughly four times those of VRC03 and NIH45-46. VRC03, 3BNC117, 1-18, and CH31 focus their epitopes more toward inner domain layer 2 and the base of the V3 loop of the adjacent trimer. This difference in strategy may ultimately determine neutralization breadth since breadth is a function of residue conservation as well as affinity.

FIG 6 Legend (Continued)
NIH45-46 [PDB accession number 5WDU], 3BNC117 [PDB accession number 5V8M], 1-18 [PDB accession number 6UDJ], and CH31 [PDB accession number 6NNJ]) on the adjacent gp120 protomer (surface representation) are shown as described above for panel C. The contacting residues are defined by a 5-Å distance criterion cutoff. All contact residues are shown in a stick representation, with framework residues in light green and CDR H1 in black.

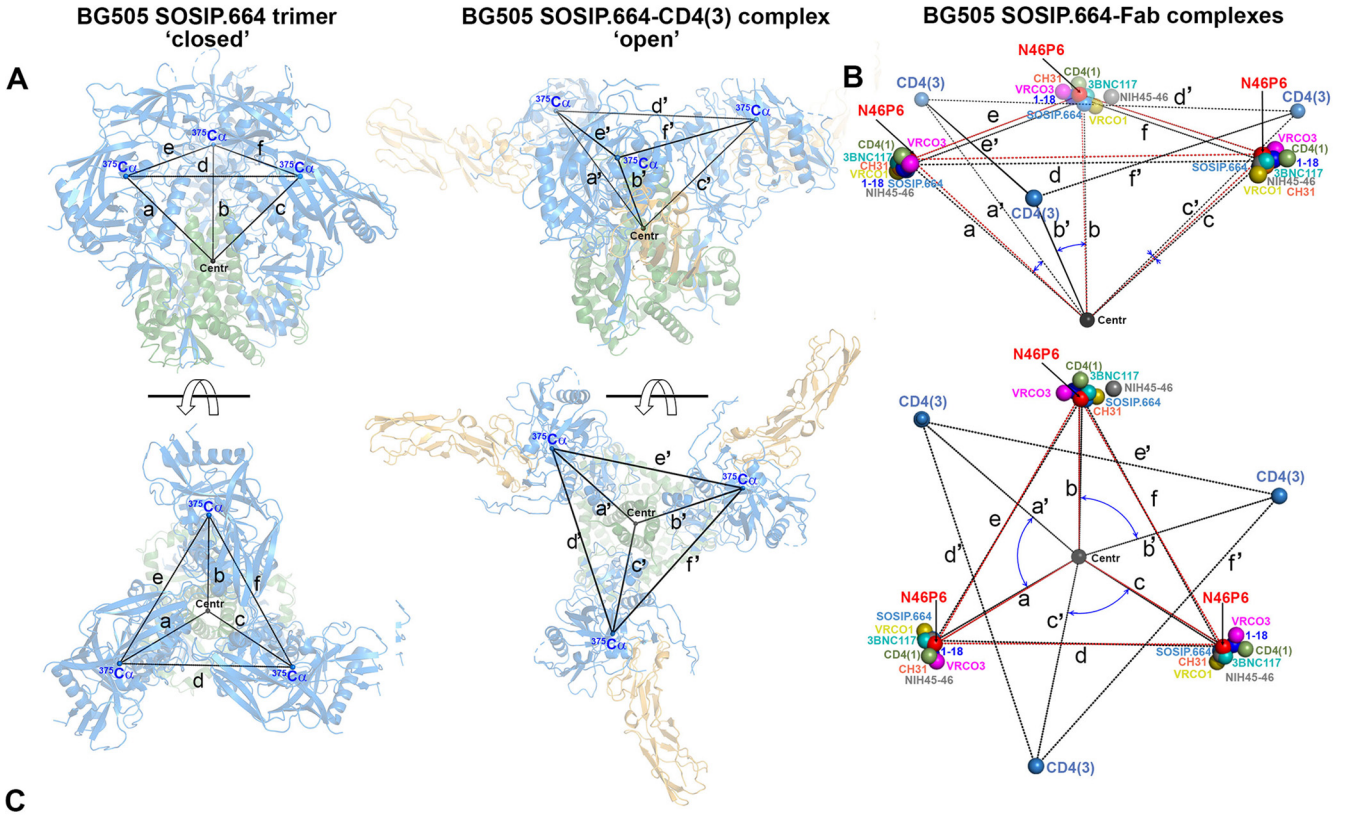

C

	a,(Å)	b,(Å)	c,(Å)	d,(Å)	e,(Å)	f,(Å)	rotation (a-a', b-b', c-c')
SOSIP.664 (PDB:4ZMJ)	45.4	45.4	45.5	54.5	54.5	54.5	0°, 0°, 0°
N49P6 Fab – BG505 SOSIP.664 (PDB:6OZ4)	46.1	46.1	46.2	54.5	54.5	54.5	1.1°, 1.1°, 1.1°
VRC01 scFv – x1193.c1 SOSIP.664 (PDB:5FYJ)	45.3	45.4	45.5	55.1	55.1	55.1	1.6°, 1.6°, 1.6°
VRC03 scFv – BG505 SOSIP.664 (PDB:6CDI)	46.7	46.7	46.7	55.6	55.6	55.5	2.7°, 2.8°, 2.8°
NIH45-46 scFv – BG505 SOSIP.664 (PDB:5WDU)	45.6	46.6	45.9	54.6	57.0	54.5	0.3°, 3.6°, 0.4°
3BNC117 scFv – BG505 SOSIP.664 (PDB:5V8M)	46.3	46.3	46.4	55.6	55.6	55.6	0.3°, 0.3°, 0.3°
CH31 scFv – BG505 SOSIP.664 (PDB:6NNJ)	45.9	46.0	46.0	55.4	55.4	55.4	0.3°, 0.3°, 0.3°
1-18 scFv – BG505 SOSIP.664 (PDB:6UDJ)	46.4	46.3	46.4	55.9	55.9	55.9	1.6°, 1.6°, 1.5°
CD4 (1) – BG505 SOSIP.664 (PDB:5U1F)	47.4	47.9	47.5	57.3	57.4	57.5	1.7°, 0.7°, 2.2°
CD4 (3) – BG505 SOSIP.664 (PDB:5VN3)	52.8	52.7	52.7	69.7	69.6	69.5	35.7°, 35.7°, 35.9°

FIG 7 Structural rearrangements of the HIV-1 Env trimer upon binding to host receptor CD4 and CD4-binding-site-specific bnAbs. (A) Overall structure of the unbound BG505 SOSIP.664 trimer (referred to as the "unbound" BG505 SOSIP conformation) (PDB accession number 4ZMJ) (left) and the trimer with 3 CD4s bound (referred to as the "soluble CD4 [sCD4]-bound" BG505 SOSIP conformation) (PDB accession number 5VN3) (right). Trimers were aligned based on the α-carbon positions of the central gp41 α7 helices, residues 570 to 595, and a center (Centr) (gray sphere) for the alignment calculated from the combined α-carbon positions. The relative position for each gp120 was then calculated based on the α-carbon position for residue 375 at the base of the CD4 Phe^{43}-binding pocket in each gp120 of the trimer ($^{375}C_\alpha$) (shown as blue spheres). The distances between the center and the $^{375}C_\alpha$ of each protomer (a, b, and c for "unbound" and a', b', and c' for "sCD4 bound") and the $^{375}C_\alpha$ atoms of neighboring protomers (d, e, and f for unbound and d', e', and f' for sCD4 bound) are shown to indicate the extent of the protomer rearrangement after CD4 binding. (B) Comparison of unbound, sCD4-bound, and bnAb-bound conformations of the HIV-1 BG505 SOSIP trimer. The BG505 SOSIP.664 complex structures (N49P6 Fab-BG505 SOSIP.664, VRC01 scFv-x1193.c1 SOSIP.664 [PDB accession number 5FYJ], VRC03 scFv-BG505 SOSIP.664 [accession number 6CDI], NIH45-46 scFv–BG505 SOSIP.664 [accession number 5WDU], 3BNC117 scFv-BG505 SOSIP.664 [accession number 5V8M], CH31 scFv-BG505 SOSIP.664 [accession number 6NNJ], 1-18 scFv–BG505 SOSIP.664 [accession number 6UDJ], and one CD4-bound BG505 SOSIP.664 [accession number 5U1F]) were aligned as described above for panel A, and the $^{375}C_\alpha$ atom of each complex is shown as colored spheres. Distances for sCD4-bound and unbound BG505 SOSIP trimers are labeled as described above for panel A, with the equivalent N49P6 distances added as red dashes. The clockwise rotation for each gp120 in the sCD4-bound trimer relative to the equivalent gp120 in the closed unbound trimer is also shown and labeled a-a', b-b', and c-c'. (C) a, b, c, d, e, and f distances and a-a', b-b', and c-c' rotation angles for each bnAb and CD4 complex relative to the unbound BG505 SOSIP trimer as shown in panel B.

DISCUSSION

The primary CD4-binding site (CD4bs), the major contact interface between the HIV-1 Env spike and host receptor CD4, can be broken down into three interacting regions, the CD4-binding loop, loop D, and loop V5 (32). Host receptor CD4 makes a number of important contacts with each of these regions that are highly conserved across HIV-1 strains (24). Broadly neutralizing CD4bs antibodies utilize many, if not all,

of these residues to achieve their neutralization breadth (6, 29, 32, 33). Increasing neutralization potency, on the other hand, also requires the use of residues outside the CD4bs for effective competition with CD4. Which residues and their conservation across HIV-1 strains are often limiting factors in an antibody's neutralization breadth, while the number and strength of the interactions outside the CD4bs are limiting factors in determining their neutralization potency.

HIV-1 has developed several strategies to prevent antibodies from binding the CD4bs and to pivot away from those that do bind to prevent neutralization. The CD4bs is recessed and shielded by heavy glycosylation on Env, which prevents all but a few antibodies from binding (34, 35). Broadly neutralizing antibodies that bind within the CD4bs have had to develop strategies to overcome this hurdle. It has been shown for the prototypical VRC01 class of CD4bs-specific bnAbs that changes, alone or in combination, in the lengths of gp120 loops D and V5 and the glycosylation pattern in loop D constitute major viral escape mechanisms through steric clashes with antibody CDR H2, the N terminus of the light chain, and/or antibody CDR L3 (36–38). VRC01-like antibodies adopt a short 5-amino-acid (aa)-long CDR L3 and often deletions in CDR L1 to accommodate changes in these regions (6, 29, 33). N49P6 together with N49P7 constitute a new branch of the VRC01-like class of CD4bs-specific bnAbs that, in addition to the strategy of shortening CDR L1 and L3, also utilize the light chain's rotation/tilt to provide additional space and prevent steric clashes with loops D and/or V5. The latter is possible due to a mutation in light chain framework region 2 (FWR2), Tyr^{36} to Cys, which allows greater mobility of the heavy and light chains relative to one other. N49P6 also contains a deletion in its CDR L1 (8 aa) in addition to the extremely short CDR L3 (5 aa) found in VRC01-like bnAbs. The combination results in a minimal light chain footprint, which can be seen by the low buried surface area (BSA), 245 $Å^2$ (157 $Å^2$ without the contribution from the Asn^{276} glycan), compared to those of most other Abs in its class (see Table S2 in the supplemental material). In addition, N49P6's CDR H2 also contains a $Pro^{60}ArgPro^{62}$ motif, which preferentially adopts a left-handed polyproline helical conformation (with phi and psi angles for Pro^{60} of −59° and 145°, Arg^{61} of −47° and −44°, and Pro^{62} of −58° and −11°, respectively) that points away from loop V5, further minimizing steric clashes with V5. Although N49P6 utilizes Asn^{276} and its attached glycan in its epitope, this interaction seems to be mainly limited to the initial *N*-acetylglucosamine. This is in contrast to VRC01 and many other VRC01-like bnAbs, which utilize more of the glycan in their epitope (39). A change in the glycan position from position 276 to position 279 in gp120, which keeps steric pressure on the CD4bs but removes many of the beneficial glycan interactions, results in neutralization resistance to many of these other CD4bs bnAbs. This change may be less of a problem for N49P6 due to its limited dependence on the Asn^{276} glycan.

The glycan at Asn^{276} prevents the binding of all but a few germ line antibody alleles to the CD4bs. Those that do either bind by utilizing a long CDR H3 to bypass light chain-mediated steric clashes or bind with one of two germ line alleles, V_H1-2 (VRC01 class) or V_H1-46 (8ANC131 class), in combination with light chains with deletions in CDR L1 and L3 (6, 29, 33). N49P6, as a member of the VRC01 class, utilizes V_H1-2 with a relatively long CDR H2 and CDR H3, composed of 17 and 20 aa, respectively. The V_H1-2 germ line gene has several characteristics of its CDR H2 that permit it to mimic CD4. For example, both the typical V_H1-2 CDR H2 and CD4 form a short antiparallel β-sheet with residues in the gp120 CD4-binding loop. In addition, V_H1-2 germ line-derived bnAbs also often mimic the salt bridge between Arg^{59} (CD4) and Asp^{368} (gp120) and utilize the hydrophobic cavity that binds Phe^{43} in CD4. The Phe^{43}-binding cavity constitutes an important anchoring point for CD4bs-specific antibodies and small-molecule CD4-mimetic compounds that rely on hydrophobic contacts with residues lining the cavity (40). N49P6 preserves many of these features along with the Arg-Asp^{368} salt bridge mediated by heavy chain framework residue Arg^{71}; however, N49P6, like N49P7, has a glycine at heavy chain position 54, which leaves the Phe^{43} cavity empty.

The Phe^{43} cavity is a key feature used by many small-molecule CD4-mimetic compounds to modulate the Env conformation and in many cases to drive Env to the CD4-bound, open conformation (40–42). To compensate for its loss, N49P6 establishes an

extensive network of interactions with loop D, loop V5, and, most importantly, the highly conserved residues within the gp120 inner domain that include inner domain layers 2 and 3. In addition, N49P6 also contacts inner domain layer 1 on the adjacent gp120 in the trimer, largely mimicking the interprotomer contact of host receptor CD4. The inner domain residues involved in the N49P6 epitope are highly conserved among HIV-1 clades, and N49P6 takes advantage of this. The mobile layers of the gp120 inner domain are involved in structural rearrangements of the HIV-1 trimer after CD4 attachment and coreceptor binding. They form the gp41-interacting face of gp120, and their conformational change serves as a driving force in trimer disassembly and cellular fusion. Their mutation comes at a fitness cost to the virus, which enables N49P6 breadth.

Finally, one of the most interesting features of how N49P6 engages HIV-1 Env is in its contact with the adjacent protomer. The mode of binding to the trimer and the scope of interprotomer contact residues largely resemble those of the interaction of host receptor CD4 in its initial binding to the HIV-1 Env trimer. Structural alignment of the N49P6-BG505 SOSIP trimer complex to the complex of the BG505 SOSIP trimer with one CD4 molecule bound (23) reveals a large overlap of the Fab/CD4 contact surface on the adjacent protomer. Other CD4bs-specific bnAbs use the adjacent protomer to increase their epitope footprint but tend to focus instead on the coreceptor-binding site at the base of the V3 loop and less on layer 1 at the site used by CD4. In this regard, N49P6 is unique in sharing many of the same contact residues used by CD4 in its initial binding to the trimer. Interestingly, it is known that following the initial contacts of one CD4 molecule to the HIV-1 BG505 SOSIP trimer, the engagement of a second and a third quickly follows, which leads to the full opening of the trimer (26). This is in contrast to the case of N49P6, where the BG505 SOSIP trimer is "locked" in the closed conformation with interprotomer distances almost identical to those of the unbound trimer.

Neutralization of the global panel of HIV-1 pseudoviruses by N49P6 is broad and potent but still leaves room for improvement, especially when IC_{80} values are used for comparison. Are there any clues from the more resistant sequences that could suggest other means to improve neutralization? Sequences from the panel that are better neutralized by N49P7 are largely conserved across N49P6 contact residues, suggesting that resistance is more subtle than those due to single point mutations (Fig. S2). Indeed, the generally high degree of conservation among epitope residues may imply that there is a large fitness cost for their mutation. Instead, one common theme among more resistant sequences in the panel and the sequences from donor N49, which are resistant to N49P6/7, is a larger V5 loop. Although most of the N49P6 epitope residues in the V5 loop reside at its base, insertions in this region may result in steric hindrance or conformational rearrangement that may lower Ab affinity. Examination of viral sequences from donor N49 shows exceptionally long V5 loops with the possible addition of a glycan, which may be a mechanism of resistance. The only other obvious difference in N49 donor sequences is the exceptionally long V1 region in the V1V2 loop (Fig. S2). To compensate, N49P7 has increased its binding to the trimer within the primary CD4-binding site. N49P6 has opted instead to increase its binding to the secondary CD4-binding site on the adjacent protomer in the trimer. Both approaches seem to have merit when applied to the global pseudovirus panel.

In conclusion, the N49 lineage of near-pan-neutralizing antibodies deconvoluted from the plasma of an HIV-1-infected individual represents a new class of CD4-binding-site-specific antibodies that we refer to as the N49P series. These antibodies omit the Phe^{43} cavity and rely strongly on the gp120 inner domain for binding to the primary gp120 protomer, and they mimic the initial contact of host receptor CD4 with the adjacent promoter of the HIV-1 Env trimer. When bound to the HIV Env trimer, N49P series antibodies lock the trimer in the closed conformation using residues from the initial contact of the CD4 receptor with the adjacent protomer in the trimer.

MATERIALS AND METHODS

Protein production and purification. N49P6 Fab was produced by papain digestion of N49P6 IgG as described previously (43, 44). BG505 SOSIP.664 was a kind gift from John Moore (Weill Cornell

Medical College, New York, NY). Complexes were made with an excess of N49P6 Fab at ratios of 1.2:1 for the gp120 complex and 3.5:1 for the SOSIP complex and then purified by gel filtration chromatography on a Superdex 200 16/60 column (GE Healthcare) equilibrated with a solution containing 10 mM Tris-HCl (pH 7.2) and 100 mM ammonium acetate. Purified complexes were concentrated to approximately 5 to 10 mg/ml for use in crystallization trials.

Neutralization assay. An HIV-1 neutralization assay was performed by measuring the reduction in luciferase expression following a single round of virus infection in TZM-bl cells as previously described (20). Briefly, mAbs were tested against murine leukemia virus (MuLV) as a negative control and a panel of pseudoviruses. Threefold serial dilutions of mAbs were tested in duplicate in 10% Dulbecco's modified Eagle growth medium (DMEM) (100 μl/well). A total of 200 50% tissue culture infective doses ($TCID_{50}$) of pseudoviruses (50 μl) were added to each well, and the plates were incubated for 1 h at 37°C. TZM-bl cells (1×10^4 cells/well in 100 μl) were then added in 10% DMEM in the presence of DEAE-dextran (Sigma, St. Louis, MO) at a final concentration of 11 μg/ml. Each well contained a final volume of 250 μl. Assay controls included replicate wells of TZM-bl cells alone (cell control), TZM-bl cells with virus (virus control), and the MuLV control. After a 48-h incubation at 37°C, 150 μl of assay medium was removed from each well, and 100 μl of Bright-Glo luciferase reagent (Promega, Madison, WI) was added to each well. The cells were allowed to lyse for 2 min, the cell lysate (150 μl) was then transferred to a 96-well black solid plate, and the luminescence intensity was measured using a Victor 3 luminometer (PerkinElmer, Waltham, MA).

Crystallization. Initial crystal screens were carried out with commercially available sparse matrix crystallization screens from Molecular Dimensions (Proplex and MacroSol) using the hanging-drop vapor diffusion method with drops of 0.5 μl protein and 0.5 μl precipitant solution. Conditions that produced crystals were optimized to produce crystals suitable for data collection. N49P6 Fab-gp120$_{93TH057}$core$_e$ complex crystals were grown from a solution containing 15% polyethylene glycol 3350 (PEG 3350) and 0.1 M Tris-HCl (pH 8.0). N49P6 Fab-BG505 SOSIP.664 complex crystals were grown from a solution containing 12% PEG 3350 and 0.1 M Tris-HCl (pH 8.0). Crystals were frozen in liquid nitrogen after a brief soak under the crystal growth conditions supplemented with 20% 2-methyl-2,4-pentanediol (MPD) before being used for data collection.

Data collection and structure solution and refinement. Diffraction data for both N49P6 complexes were collected at the Stanford Synchrotron Radiation Light Source (SSRL) at beamline BL12-2 equipped with a Dectris Pilatus area detector. N49P6 Fab-gp120$_{93TH057}$core$_e$ crystals belong to orthorhombic space group $P2_12_12_1$ with unit cell parameters of $a = 65.4$, $b = 80.8$, and $c = 195.2$ Å and one N49P6 Fab-gp120$_{93TH057}$core$_e$ complex present in the asymmetric unit (ASU). N49P6 Fab-BG505 SOSIP.664 complex crystals belong to cubic space group $P2_13$ with unit cell parameters $a = b = c = 164.7$ Å and one-third of the N49P6 Fab-BG505 SOSIP.664 trimer present in the ASU. Data were processed and reduced with HKL2000 (45). The N49P6 Fab-gp120$_{93TH057}$core$_e$ complex structure was solved by molecular replacement with Phaser (46) from the CCP4 suite (47) based on the coordinates of the N49P7 Fab-gp120$_{93TH057}$core$_e$ complex (PDB accession number 6BCK). The N49P6 Fab-BG505 SOSIP.664 complex was solved using coordinates of gp120 and gp41 from BG505 SOSIP.664 in complex with PGT122 and 35O22 Fabs (PDB accession number 4TVP) and the refined N49P6 Fab coordinates from the N49P6 gp120 complex. Refinement was done with Refmac (48) and/or Phenix (49). Refinement was coupled with manual refitting and rebuilding in COOT (50). The N49P6 Fab-gp120$_{93TH057}$core$_e$ complex diffracted to 2.55 Å and was refined to an R-factor of 0.219 and an R_{free} of 0.273. The N49P6 Fab-BG505 SOSIP.664 complex diffracted to 4.05 Å and was refined to an R-factor of 0.255 and an R_{free} of 0.315. Data collection/refinement statistics are shown in Table 1.

Structure validation and analysis. The quality of the final refined model was monitored using the program MolProbity (51). Structural alignments were performed using the program lsqkab from the CCP4 suite. The PISA Web server (52) was used to determine contact surfaces and interface residues. All illustrations were prepared with the PyMOL Molecular Graphics suite (http://pymol.org) (DeLano Scientific, San Carlos, CA, USA).

Availability of data. The data sets generated and/or analyzed during the current study are available in the Protein Data Bank (PDB) repository under accession numbers 6OZ2 and 6OZ4.

SUPPLEMENTAL MATERIAL

Supplemental material is available online only.

FIG S1, TIF file, 1.5 MB.

FIG S2, TIF file, 1.1 MB.

TABLE S1, DOCX file, 0.02 MB.

TABLE S2, DOCX file, 0.02 MB.

ACKNOWLEDGMENTS

Funding for this study was provided by National Institutes of Health grants R01 AI116274 to M.P.; R01 AI129769 to M.P.; R01 AI147870, IBX004525, and OPP1197311 to M.M.S.; and P01 AI120756 to M.P. and Georgia Tomaras. Use of the Stanford Synchrotron Radiation Light Source, SLAC National Accelerator Laboratory, is supported by the U.S. Department of Energy, Office of Science, Office of Basic Energy Sciences, under contract number DE-AC02-76SF00515. The SSRL Structural Molecular Biology Program is supported

by the DOE Office of Biological and Environmental Research and by the National Institutes of Health, National Institute of General Medical Sciences. The funders had no role in study design, data collection and analysis, decision to publish, or preparation of the manuscript, and the contents of this publication are solely the responsibility of the authors.

The views expressed in this presentation are those of the authors and do not reflect the official policy or position of the Uniformed Services University, U.S. Army, the Department of Defense, or the U.S. Government.

We declare that we have no competing interests.

W.D.T., D.N.N., and M.P. designed, performed research, and analyzed the data; Z.R.T. and M.M.S. isolated N49P6 antibody and performed neutralization assays; W.D.T., D.N.N., and M.P. wrote the manuscript; and all authors provided comments or revisions.

REFERENCES

1. Stefic K, Bouvin-Pley M, Braibant M, Barin F. 2019. Impact of HIV-1 diversity on its sensitivity to neutralization. Vaccines (Basel) 7:74. https://doi.org/10.3390/vaccines7030074.
2. Wu X, Yang ZY, Li Y, Hogerkorp CM, Schief WR, Seaman MS, Zhou T, Schmidt SD, Wu L, Xu L, Longo NS, McKee K, O'Dell S, Louder MK, Wycuff DL, Feng Y, Nason M, Doria-Rose N, Connors M, Kwong PD, Roederer M, Wyatt RT, Nabel GJ, Mascola JR. 2010. Rational design of envelope identifies broadly neutralizing human monoclonal antibodies to HIV-1. Science 329:856–861. https://doi.org/10.1126/science.1187659.
3. Trkola A, Pomales AB, Yuan H, Korber B, Maddon PJ, Allaway GP, Katinger H, Barbas CF, III, Burton DR, Ho DD, Moore JP. 1995. Cross-clade neutralization of primary isolates of human immunodeficiency virus type 1 by human monoclonal antibodies and tetrameric CD4-IgG. J Virol 69:6609–6617. https://doi.org/10.1128/JVI.69.11.6609-6617.1995.
4. Gray ES, Madiga MC, Moore PL, Mlisana K, Abdool Karim SS, Binley JM, Shaw GM, Mascola JR, Morris L. 2009. Broad neutralization of human immunodeficiency virus type 1 mediated by plasma antibodies against the gp41 membrane proximal external region. J Virol 83:11265–11274. https://doi.org/10.1128/JVI.01359-09.
5. Huang J, Kang BH, Pancera M, Lee JH, Tong T, Feng Y, Imamichi H, Georgiev IS, Chuang GY, Druz A, Doria-Rose NA, Laub L, Sliepen K, van Gils MJ, de la Pena AT, Derking R, Klasse PJ, Migueles SA, Bailer RT, Alam M, Pugach P, Haynes BF, Wyatt RT, Sanders RW, Binley JM, Ward AB, Mascola JR, Kwong PD, Connors M. 2014. Broad and potent HIV-1 neutralization by a human antibody that binds the gp41-gp120 interface. Nature 515:138–142. https://doi.org/10.1038/nature13601.
6. Zhou T, Lynch RM, Chen L, Acharya P, Wu X, Doria-Rose NA, Joyce MG, Lingwood D, Soto C, Bailer RT, Ernandes MJ, Kong R, Longo NS, Louder MK, McKee K, O'Dell S, Schmidt SD, Tran L, Yang Z, Druz A, Luongo TS, Moquin S, Srivatsan S, Yang Y, Zhang B, Zheng A, Pancera M, Kirys T, Georgiev IS, Gindin T, Peng H-P, Yang A-S, NISC Comparative Sequencing Program, Mullikin JC, Gray MD, Stamatatos L, Burton DR, Koff WC, Cohen MS, Haynes BF, Casazza JP, Connors M, Corti D, Lanzavecchia A, Sattentau QJ, Weiss RA, West AP, Jr, Bjorkman PJ, Scheid JF, Nussenzweig MC, Shapiro L, et al. 2015. Structural repertoire of HIV-1-neutralizing antibodies targeting the CD4 supersite in 14 donors. Cell 161:1280–1292. https://doi.org/10.1016/j.cell.2015.05.007.
7. Sok D, Burton DR. 2018. Recent progress in broadly neutralizing antibodies to HIV. Nat Immunol 19:1179–1188. https://doi.org/10.1038/s41590-018-0235-7.
8. Dashti A, DeVico AL, Lewis GK, Sajadi MM. 2019. Broadly neutralizing antibodies against HIV: back to blood. Trends Mol Med 25:228–240. https://doi.org/10.1016/j.molmed.2019.01.007.
9. Huang J, Kang BH, Ishida E, Zhou T, Griesman T, Sheng Z, Wu F, Doria-Rose NA, Zhang B, McKee K, O'Dell S, Chuang GY, Druz A, Georgiev IS, Schramm CA, Zheng A, Joyce MG, Asokan M, Ransier A, Darko S, Migueles SA, Bailer RT, Louder MK, Alam SM, Parks R, Kelsoe G, Von Holle T, Haynes BF, Douek DC, Hirsch V, Seaman MS, Shapiro L, Mascola JR, Kwong PD, Connors M. 2016. Identification of a CD4-binding-site antibody to HIV that evolved near-pan neutralization breadth. Immunity 45:1108–1121. https://doi.org/10.1016/j.immuni.2016.10.027.
10. Schommers P, Gruell H, Abernathy ME, Tran MK, Dingens AS, Gristick HB, Barnes CO, Schoofs T, Schlotz M, Vanshylla K, Kreer C, Weiland D, Holtick U, Scheid C, Valter MM, van Gils MJ, Sanders RW, Vehreschild JJ, Cornely OA, Lehmann C, Fatkenheuer G, Seaman MS, Bloom JD, Bjorkman PJ, Klein F. 2020. Restriction of HIV-1 escape by a highly broad and potent neutralizing antibody. Cell 180:471–489.e22. https://doi.org/10.1016/j.cell.2020.01.010.
11. Scheid JF, Mouquet H, Ueberheide B, Diskin R, Klein F, Oliveira TY, Pietzsch J, Fenyo D, Abadir A, Velinzon K, Hurley A, Myung S, Boulad F, Poignard P, Burton DR, Pereyra F, Ho DD, Walker BD, Seaman MS, Bjorkman PJ, Chait BT, Nussenzweig MC. 2011. Sequence and structural convergence of broad and potent HIV antibodies that mimic CD4 binding. Science 333:1633–1637. https://doi.org/10.1126/science.1207227.
12. Rudicell RS, Kwon YD, Ko S-Y, Pegu A, Louder MK, Georgiev IS, Wu X, Zhu J, Boyington JC, Chen X, Shi W, Yang Z-Y, Doria-Rose NA, McKee K, O'Dell S, Schmidt SD, Chuang G-Y, Druz A, Soto C, Yang Y, Zhang B, Zhou T, Todd J-P, Lloyd KE, Eudailey J, Roberts KE, Donald BR, Bailer RT, Ledgerwood J, NISC Comparative Sequencing Program, Mullikin JC, Shapiro L, Koup RA, Graham BS, Nason MC, Connors M, Haynes BF, Rao SS, Roederer M, Kwong PD, Mascola JR, Nabel GJ. 2014. Enhanced potency of a broadly neutralizing HIV-1 antibody in vitro improves protection against lentiviral infection in vivo. J Virol 88:12669–12682. https://doi.org/10.1128/JVI.02213-14.
13. Halliley JL, Tipton CM, Liesveld J, Rosenberg AF, Darce J, Gregoretti IV, Popova L, Kaminiski D, Fucile CF, Albizua I, Kyu S, Chiang KY, Bradley KT, Burack R, Slifka M, Hammarlund E, Wu H, Zhao L, Walsh EE, Falsey AR, Randall TD, Cheung WC, Sanz I, Lee FE. 2015. Long-lived plasma cells are contained within the CD19(−)CD38(hi)CD138(+) subset in human bone marrow. Immunity 43:132–145. https://doi.org/10.1016/j.immuni.2015.06.016.
14. Briney BS, Willis JR, Finn JA, McKinney BA, Crowe JE, Jr. 2014. Tissue-specific expressed antibody variable gene repertoires. PLoS One 9:e100839. https://doi.org/10.1371/journal.pone.0100839.
15. Walker LM, Phogat SK, Chan-Hui P-Y, Wagner D, Phung P, Goss JL, Wrin T, Simek MD, Fling S, Mitcham JL, Lehrman JK, Priddy FH, Olsen OA, Frey SM, Hammond PW, Protocol G Principal Investigators, Kaminsky S, Zamb T, Moyle M, Koff WC, Poignard P, Burton DR. 2009. Broad and potent neutralizing antibodies from an African donor reveal a new HIV-1 vaccine target. Science 326:285–289. https://doi.org/10.1126/science.1178746.
16. Scheid JF, Mouquet H, Feldhahn N, Seaman MS, Velinzon K, Pietzsch J, Ott RG, Anthony RM, Zebroski H, Hurley A, Phogat A, Chakrabarti B, Li Y, Connors M, Pereyra F, Walker BD, Wardemann H, Ho D, Wyatt RT, Mascola JR, Ravetch JV, Nussenzweig MC. 2009. Broad diversity of neutralizing antibodies isolated from memory B cells in HIV-infected individuals. Nature 458:636–640. https://doi.org/10.1038/nature07930.
17. Guan Y, Sajadi MM, Kamin-Lewis R, Fouts TR, Dimitrov A, Zhang Z, Redfield RR, DeVico AL, Gallo RC, Lewis GK. 2009. Discordant memory B cell and circulating anti-Env antibody responses in HIV-1 infection. Proc Natl Acad Sci U S A 106:3952–3957. https://doi.org/10.1073/pnas.0813392106.
18. Sajadi MM, Farshidpour M, Brown EP, Ouyang X, Seaman MS, Pazgier M, Ackerman ME, Robinson H, Tomaras G, Parsons MS, Charurat M, DeVico AL, Redfield RR, Lewis GK. 2016. Lambda light chain bias associated with enhanced binding and function of anti-HIV Env glycoprotein antibodies. J Infect Dis 213:156–164. https://doi.org/10.1093/infdis/jiv448.
19. Sajadi MM, Lewis GK, Seaman MS, Guan Y, Redfield RR, DeVico AL. 2012. Signature biochemical properties of broadly cross-reactive HIV-1 neutralizing antibodies in human plasma. J Virol 86:5014–5025. https://doi.org/10.1128/JVI.06547-11.
20. Sajadi MM, Dashti A, Rikhtegaran Tehrani Z, Tolbert WD, Seaman MS, Ouyang X, Gohain N, Pazgier M, Kim D, Cavet G, Yared J, Redfield RR, Lewis GK, DeVico AL. 2018. Identification of near-pan-neutralizing

antibodies against HIV-1 by deconvolution of plasma humoral responses. Cell 173:1783–1795.e14. https://doi.org/10.1016/j.cell.2018.03.061.
21. Desormeaux A, Coutu M, Medjahed H, Pacheco B, Herschhorn A, Gu C, Xiang SH, Mao Y, Sodroski J, Finzi A. 2013. The highly conserved layer-3 component of the HIV-1 gp120 inner domain is critical for CD4-required conformational transitions. J Virol 87:2549–2562. https://doi.org/10.1128/JVI.03104-12.
22. Finzi A, Xiang SH, Pacheco B, Wang L, Haight J, Kassa A, Danek B, Pancera M, Kwong PD, Sodroski J. 2010. Topological layers in the HIV-1 gp120 inner domain regulate gp41 interaction and CD4-triggered conformational transitions. Mol Cell 37:656–667. https://doi.org/10.1016/j.molcel.2010.02.012.
23. Liu Q, Acharya P, Dolan MA, Zhang P, Guzzo C, Lu J, Kwon A, Gururani D, Miao H, Bylund T, Chuang GY, Druz A, Zhou T, Rice WJ, Wigge C, Carragher B, Potter CS, Kwong PD, Lusso P. 2017. Quaternary contact in the initial interaction of CD4 with the HIV-1 envelope trimer. Nat Struct Mol Biol 24:370–378. https://doi.org/10.1038/nsmb.3382.
24. Kwong PD, Wyatt R, Robinson J, Sweet RW, Sodroski J, Hendrickson WA. 1998. Structure of an HIV gp120 envelope glycoprotein in complex with the CD4 receptor and a neutralizing human antibody. Nature 393:648–659. https://doi.org/10.1038/31405.
25. Agrawal P, DeVico AL, Foulke JS, Jr, Lewis GK, Pazgier M, Ray K. 2019. Stoichiometric analyses of soluble CD4 to native-like HIV-1 envelope by single-molecule fluorescence spectroscopy. Cell Rep 29:176–186.e4. https://doi.org/10.1016/j.celrep.2019.08.074.
26. Ozorowski G, Pallesen J, de Val N, Lyumkis D, Cottrell CA, Torres JL, Copps J, Stanfield RL, Cupo A, Pugach P, Moore JP, Wilson IA, Ward AB. 2017. Open and closed structures reveal allostery and pliability in the HIV-1 envelope spike. Nature 547:360–363. https://doi.org/10.1038/nature23010.
27. Shaik MM, Peng H, Lu J, Rits-Volloch S, Xu C, Liao M, Chen B. 2019. Structural basis of coreceptor recognition by HIV-1 envelope spike. Nature 565:318–323. https://doi.org/10.1038/s41586-018-0804-9.
28. Stewart-Jones GB, Soto C, Lemmin T, Chuang GY, Druz A, Kong R, Thomas PV, Wagh K, Zhou T, Behrens AJ, Bylund T, Choi CW, Davison JR, Georgiev IS, Joyce MG, Kwon YD, Pancera M, Taft J, Yang Y, Zhang B, Shivatare SS, Shivatare VS, Lee CC, Wu CY, Bewley CA, Burton DR, Koff WC, Connors M, Crispin M, Baxa U, Korber BT, Wong CH, Mascola JR, Kwong PD. 2016. Trimeric HIV-1-Env structures define glycan shields from clades A, B, and G. Cell 165:813–826. https://doi.org/10.1016/j.cell.2016.04.010.
29. Wu X, Zhou T, Zhu J, Zhang B, Georgiev I, Wang C, Chen X, Longo NS, Louder M, McKee K, O'Dell S, Perfetto S, Schmidt SD, Shi W, Wu L, Yang Y, Yang Z-Y, Yang Z, Zhang Z, Bonsignori M, Crump JA, Kapiga SH, Sam NE, Haynes BF, Simek M, Burton DR, Koff WC, Doria-Rose NA, Connors M, NISC Comparative Sequencing Program, Mullikin JC, Nabel GJ, Roederer M, Shapiro L, Kwong PD, Mascola JR. 2011. Focused evolution of HIV-1 neutralizing antibodies revealed by structures and deep sequencing. Science 333:1593–1602. https://doi.org/10.1126/science.1207532.
30. Xu K, Acharya P, Kong R, Cheng C, Chuang G-Y, Liu K, Louder MK, O'Dell S, Rawi R, Sastry M, Shen C-H, Zhang B, Zhou T, Asokan M, Bailer RT, Chambers M, Chen X, Choi CW, Dandey VP, Doria-Rose NA, Druz A, Eng ET, Farney SK, Foulds KE, Geng H, Georgiev IS, Gorman J, Hill KR, Jafari AJ, Kwon YD, Lai Y-T, Lemmin T, McKee K, Ohr TY, Ou L, Peng D, Rowshan AP, Sheng Z, Todd J-P, Tsybovsky Y, Viox EG, Wang Y, Wei H, Yang Y, Zhou AF, Chen R, Yang L, Scorpio DG, McDermott AB, Shapiro L, et al. 2018. Epitope-based vaccine design yields fusion peptide-directed antibodies that neutralize diverse strains of HIV-1. Nat Med 24:857–867. https://doi.org/10.1038/s41591-018-0042-6.
31. Lee JH, Andrabi R, Su CY, Yasmeen A, Julien JP, Kong L, Wu NC, McBride R, Sok D, Pauthner M, Cottrell CA, Nieusma T, Blattner C, Paulson JC, Klasse PJ, Wilson IA, Burton DR, Ward AB. 2017. A broadly neutralizing antibody targets the dynamic HIV envelope trimer apex via a long, rigidified, and anionic beta-hairpin structure. Immunity 46:690–702. https://doi.org/10.1016/j.immuni.2017.03.017.
32. Zhou T, Georgiev I, Wu X, Yang ZY, Dai K, Finzi A, Kwon YD, Scheid JF, Shi W, Xu L, Yang Y, Zhu J, Nussenzweig MC, Sodroski J, Shapiro L, Nabel GJ, Mascola JR, Kwong PD. 2010. Structural basis for broad and potent neutralization of HIV-1 by antibody VRC01. Science 329:811–817. https://doi.org/10.1126/science.1192819.
33. Scharf L, West AP, Sievers SA, Chen C, Jiang S, Gao H, Gray MD, McGuire AT, Scheid JF, Nussenzweig MC, Stamatatos L, Bjorkman PJ. 2016. Structural basis for germline antibody recognition of HIV-1 immunogens. Elife 5:e13783. https://doi.org/10.7554/eLife.13783.
34. Zhou T, Doria-Rose NA, Cheng C, Stewart-Jones GBE, Chuang GY, Chambers M, Druz A, Geng H, McKee K, Kwon YD, O'Dell S, Sastry M, Schmidt SD, Xu K, Chen L, Chen RE, Louder MK, Pancera M, Wanninger TG, Zhang B, Zheng A, Farney SK, Foulds KE, Georgiev IS, Joyce MG, Lemmin T, Narpala S, Rawi R, Soto C, Todd JP, Shen CH, Tsybovsky Y, Yang Y, Zhao P, Haynes BF, Stamatatos L, Tiemeyer M, Wells L, Scorpio DG, Shapiro L, McDermott AB, Mascola JR, Kwong PD. 2017. Quantification of the impact of the HIV-1-glycan shield on antibody elicitation. Cell Rep 19:719–732. https://doi.org/10.1016/j.celrep.2017.04.013.
35. Gristick HB, Wang H, Bjorkman PJ. 2017. X-ray and EM structures of a natively glycosylated HIV-1 envelope trimer. Acta Crystallogr D Struct Biol 73:822–828. https://doi.org/10.1107/S2059798317013353.
36. Lynch RM, Wong P, Tran L, O'Dell S, Nason MC, Li Y, Wu X, Mascola JR. 2015. HIV-1 fitness cost associated with escape from the VRC01 class of CD4 binding site neutralizing antibodies. J Virol 89:4201–4213. https://doi.org/10.1128/JVI.03608-14.
37. Dingens AS, Haddox HK, Overbaugh J, Bloom JD. 2017. Comprehensive mapping of HIV-1 escape from a broadly neutralizing antibody. Cell Host Microbe 21:777–787.e4. https://doi.org/10.1016/j.chom.2017.05.003.
38. Otsuka Y, Schmitt K, Quinlan BD, Gardner MR, Alfant B, Reich A, Farzan M, Choe H. 2018. Diverse pathways of escape from all well-characterized VRC01-class broadly neutralizing HIV-1 antibodies. PLoS Pathog 14:e1007238. https://doi.org/10.1371/journal.ppat.1007238.
39. Balla-Jhagjhoorsingh SS, Corti D, Heyndrickx L, Willems E, Vereecken K, Davis D, Vanham G. 2013. The N276 glycosylation site is required for HIV-1 neutralization by the CD4 binding site specific HJ16 monoclonal antibody. PLoS One 8:e68863. https://doi.org/10.1371/journal.pone.0068863.
40. Grupping K, Selhorst P, Michiels J, Vereecken K, Heyndrickx L, Kessler P, Vanham G, Martin L, Arien KK. 2012. MiniCD4 protein resistance mutations affect binding to the HIV-1 gp120 CD4 binding site and decrease entry efficiency. Retrovirology 9:36. https://doi.org/10.1186/1742-4690-9-36.
41. Jette CA, Barnes CO, Kirk SM, Melillo B, Smith AB, Bjorkman PJ. 2020. Cryo-EM structures of HIV-1 trimer bound to CD4-mimetics M48U1 and BNM-III-170 adopt a CD4-bound open conformation. bioRxiv https://doi.org/10.1101/2020.08.21.261974.
42. Prévost J, Tolbert WD, Medjahed H, Sherburn RT, Madani N, Zoubchenok D, Gendron-Lepage G, Gaffney AE, Grenier MC, Kirk S, Vergara N, Han C, Mann BT, Chénine AL, Ahmed A, Chaiken I, Kirchhoff F, Hahn BH, Haim H, Abrams CF, Smith AB, III, Sodroski J, Pazgier M, Finzi A. 2020. The HIV-1 Env gp120 inner domain shapes the Phe43 cavity and the CD4 binding site. mBio 11:e00280-20. https://doi.org/10.1128/mBio.00280-20.
43. Acharya P, Tolbert WD, Gohain N, Wu X, Yu L, Liu T, Huang W, Huang CC, Kwon YD, Louder RK, Luongo TS, McLellan JS, Pancera M, Yang Y, Zhang B, Flinko R, Foulke JS, Jr, Sajadi MM, Kamin-Lewis R, Robinson JE, Martin L, Kwong PD, Guan Y, DeVico AL, Lewis GK, Pazgier M. 2014. Structural definition of an antibody-dependent cellular cytotoxicity response implicated in reduced risk for HIV-1 infection. J Virol 88:12895–12906. https://doi.org/10.1128/JVI.02194-14.
44. Gohain N, Tolbert WD, Acharya P, Yu L, Liu T, Zhao P, Orlandi C, Visciano ML, Kamin-Lewis R, Sajadi MM, Martin L, Robinson JE, Kwong PD, DeVico AL, Ray K, Lewis GK, Pazgier M. 2015. Cocrystal structures of antibody N60-i3 and antibody JR4 in complex with gp120 define more cluster A epitopes involved in effective antibody-dependent effector function against HIV-1. J Virol 89:8840–8854. https://doi.org/10.1128/JVI.01232-15.
45. Otwinowski Z, Minor W. 1997. Processing of X-ray diffraction data collected in oscillation mode. Methods Enzymol 276:307–326. https://doi.org/10.1016/S0076-6879(97)76066-X.
46. McCoy AJ. 2007. Solving structures of protein complexes by molecular replacement with Phaser. Acta Crystallogr D Biol Crystallogr 63:32–41. https://doi.org/10.1107/S0907444906045975.
47. Collaborative Computational Project, Number 4. 1994. The CCP4 suite: programs for protein crystallography. Acta Crystallogr D Biol Crystallogr 50:760–763. https://doi.org/10.1107/S0907444994003112.
48. Murshudov GN, Vagin AA, Dodson EJ. 1997. Refinement of macromolecular structures by the maximum-likelihood method. Acta Crystallogr D Biol Crystallogr 53:240–255. https://doi.org/10.1107/S0907444996012255.
49. Adams PD, Grosse-Kunstleve RW, Hung LW, Ioerger TR, McCoy AJ, Moriarty NW, Read RJ, Sacchettini JC, Sauter NK, Terwilliger TC. 2002. PHENIX: building new software for automated crystallographic structure determination. Acta Crystallogr D Biol Crystallogr 58:1948–1954. https://doi.org/10.1107/s0907444902016657.
50. Emsley P, Cowtan K. 2004. Coot: model-building tools for molecular graphics. Acta Crystallogr D Biol Crystallogr 60:2126–2132. https://doi.org/10.1107/S0907444904019158.

51. Davis IW, Murray LW, Richardson JS, Richardson DC. 2004. MOLPROBITY: structure validation and all-atom contact analysis for nucleic acids and their complexes. Nucleic Acids Res 32:W615–W619. https://doi.org/10.1093/nar/gkh398.
52. Krissinel E, Henrick K. 2007. Inference of macromolecular assemblies from crystalline state. J Mol Biol 372:774–797. https://doi.org/10.1016/j.jmb.2007.05.022.
53. Weiss MS. 2001. Global indicators of X-ray data quality. J Appl Crystallogr 34:130–135. https://doi.org/10.1107/S0021889800018227.
54. Karplus PA, Diederichs K. 2012. Linking crystallographic model and data quality. Science 336:1030–1033. https://doi.org/10.1126/science.1218231.
55. Popov AN, Bourenkov GP. 2003. Choice of data-collection parameters based on statistic modelling. Acta Crystallogr D Biol Crystallogr 59:1145–1153. https://doi.org/10.1107/s0907444903008163.